

SN 2009bb: a Peculiar Broad-Lined Type Ic Supernova^{1,2}

Giuliano Pignata,^{3,4} Maximilian Stritzinger,^{5,6,7} Alicia Soderberg,⁸ Paolo Mazzali,^{9,10,11}

M. M. Phillips,⁵ Nidia Morrell,⁵ J. P. Anderson,⁴ Luis Boldt,⁵ Abdo Campillay,⁵

Carlos Contreras,^{5,12} Gastón Folatelli,⁴ Francisco Förster,⁴ Sergio González,⁵

Mario Hamuy,⁴ Wojtek Krzeminski,⁵ José Maza,⁴ Miguel Roth,⁵ Francisco Salgado,⁵

Emily M. Levesque,¹³ Armin Rest,¹⁴ J. Adam Crain,¹⁵ Andrew C. Foster,¹⁵

Joshua B. Haislip,¹⁵ Kevin M. Ivarsen,¹⁵ Aaron P. LaCluyze,¹⁵ Melissa C. Nysewander,¹⁵

Daniel E. Reichart¹⁵

Received _____; accepted _____

¹This paper includes data gathered with the 6.5-m Magellan Telescopes located at Las Campanas Observatory, Chile.

²Based on observations obtained at the Gemini Observatory, Cerro Pachon, Chile (Gemini Programs GS-2009A-Q-17 and GS-2009A-Q-43).

³Departamento de Ciencias Físicas, Universidad Andrés Bello, Avda. República 252, Santiago, Chile

⁴Departamento de Astronomía, Universidad de Chile, Casilla 36-D, Santiago, Chile.

⁵Las Campanas Observatory, Carnegie Observatories, Casilla 601, La Serena, Chile.

⁶Dark Cosmology Centre, Niels Bohr Institute, University of Copenhagen, Juliane Maries Vej 30, 2100 Copenhagen Ø, Denmark.

⁷The Oskar Klein Centre, Department of Astronomy, Stockholm University, AlbaNova, 10691 Stockholm, Sweden.

⁸Harvard-Smithsonian Center for Astrophysics, 60 Garden Street, Cambridge, MA 02138, USA.

⁹Max-Planck-Institut für Astrophysik, Karl-Schwarzschild-Strasse 1, 85741 Garching, Germany.

¹⁰Scuola Normale Superiore, Piazza Cavalieri 7, 56127 Pisa, Italy.

¹¹INAF Oss. Astron. Padova, vicolo dell'Osservatorio 5, 35122 Padova, Italy

¹²Centre for Astrophysics & Supercomputing, Swinburne University of Technology, P.O. Box 218, Victoria 3122, Australia.

¹³Institute for Astronomy, University of Hawaii, 2680 Woodlawn Drive, Honolulu, HI 96822, USA

¹⁴Department of Physics, Harvard University, 17 Oxford Street, Cambridge, MA 02138, USA

¹⁵University of North Carolina at Chapel Hill, Campus Box 3255, Chapel Hill, NC 27599-

ABSTRACT

Ultraviolet, optical, and near-infrared photometry and optical spectroscopy of the broad-lined Type Ic supernova (SN) 2009bb are presented, following the flux evolution from -10 to $+285$ days past B -band maximum. Thanks to the very early discovery, it is possible to place tight constraints on the SN explosion epoch. The expansion velocities measured from near maximum spectra are found to be only slightly smaller than those measured from spectra of the prototype broad-lined SN 1998bw associated with GRB 980425. Fitting an analytical model to the pseudo-bolometric light curve of SN 2009bb suggests that $4.1 \pm 1.9 M_{\odot}$ of material was ejected with $0.22 \pm 0.06 M_{\odot}$ of it being ^{56}Ni . The resulting kinetic energy is $1.8 \pm 0.7 \times 10^{52}$ erg. This, together with an absolute peak magnitude of $M_B = -18.36 \pm 0.44$, places SN 2009bb on the energetic and luminous end of the broad-lined Type Ic (SN Ic) sequence. Detection of helium in the early time optical spectra accompanied with strong radio emission, and high metallicity of its environment makes SN 2009bb a peculiar object. Similar to the case for GRBs, we find that the bulk explosion parameters of SN 2009bb cannot account for the copious energy coupled to relativistic ejecta, and conclude that another energy reservoir (a central engine) is required to power the radio emission. Nevertheless, the analysis of the SN 2009bb nebular spectrum suggests that the failed GRB detection is not imputable to a large angle between the line-of-sight and the GRB beamed radiation. Therefore, if a GRB was produced during the SN 2009bb explosion, it was below the threshold of the current generation of γ -ray instruments.

Subject headings: galaxies: individual (NGC 3278) — supernovae: general — supernovae: individual (SN 2009bb)

1. Introduction

A decade has passed since the discovery of the association between the long-duration Gamma Ray Burst (GRB) 980425 and the broad-lined Type Ic SN 1998bw (Galama et al. 1998; Patat et al. 2001). This realization led to a renewed interest in the study of stripped-envelope core-collapse supernovae (SNe). In the case of SN 1998bw, the high kinetic energy inferred from the expansion velocity coupled with an exceedingly high luminosity and strong radio emission set it apart from all other previously-observed core-collapse SNe. Since then these attributes have been shown also by other GRB-related SNe like SN 2003lw (Malesani et al. 2004; Gal-Yam et al. 2004) and SN 2003dh (Stanek et al. 2003; Hjorth et al. 2003; Matheson et al. 2003). The X-ray flash SN 2006aj (Pian et al. 2006; Modjaz et al. 2006; Sollerman et al. 2006; Ferrero et al. 2006; Kocevski et al. 2007), was not as extreme as the previous SNe, nevertheless it shows expansion velocity much higher than normal Type Ic SNe.

In addition to these GRB related, broad-lined SNe Ic, there have also been a number of other discovered broad-lined events that are apparently not associated with a GRB, e.g. SN 1997ef, (Matheson et al. 2001), SN 2002ap (Gal-Yam, Ofek & Shemmer 2002; Foley et al. 2003; Yoshii et al. 2003), SN 2003jd (Valenti et al. 2008) and SN 2007ru (Sahu et al. 2009). Recently two other broad-lined events have been published that underscore the heterogeneous nature of this family of SNe. In particular, early phase spectra of the broad-lined Type Ic SN 2007bg exhibit evidence of *helium* (Young et al. 2010), while Hamuy et al. (2009) have presented the first case of a *hydrogen-rich* broad-lined Type IIb SN 2003bg.

In this paper we present ultraviolet, optical and near-infrared photometry and optical spectroscopy of SN 2009bb. This object was discovered by the CHilean Automated Supernova sEarch CHASE (Pignata et al. 2009a) on 2009 March 21.11 UT with the

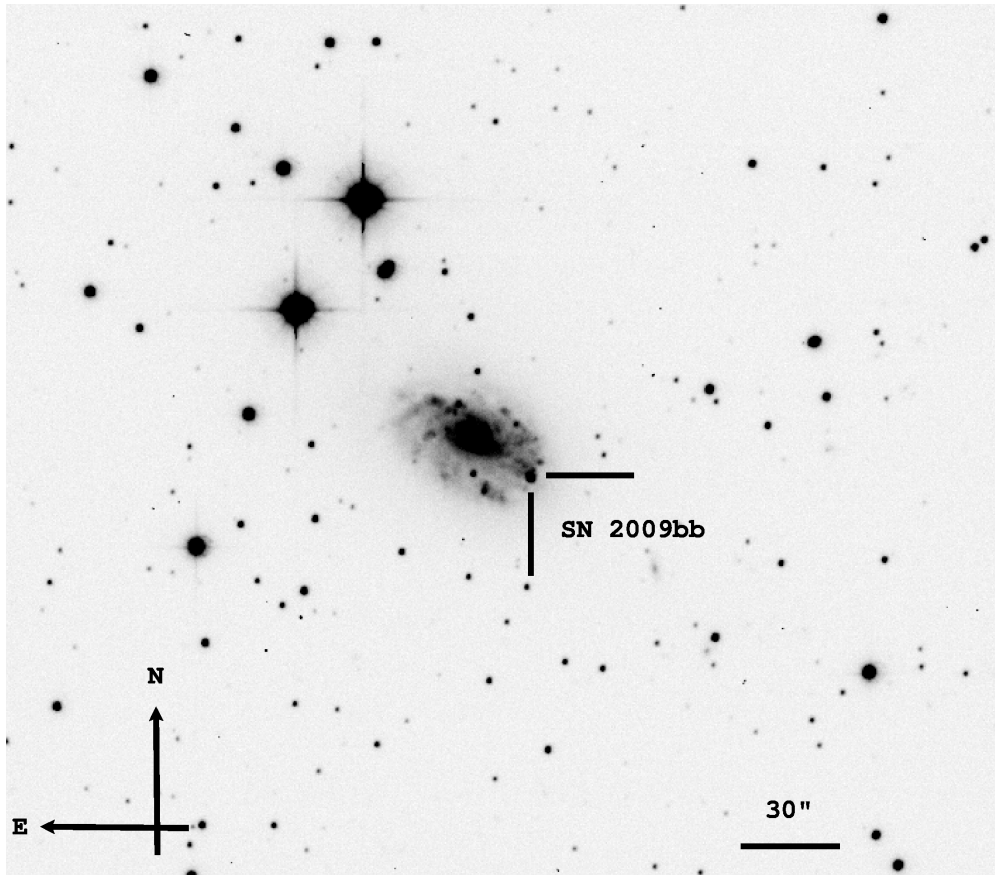


Fig. 1.— Finder chart for SN 2009bb obtained from a *V* band image acquired on 2009 March 30 with the 1.0 m Swope telescope at Las Campanas Observatory.

Panchromatic Robotic Optical Monitoring and Polarimetry Telescope (PROMPT) 3 at the Cerro Tololo Inter-American Observatory (CTIO).¹⁶ The SN is located (see Figure 1) at $\alpha = 10^h31^m33^s.87$ and $\delta = -39^\circ57'30.0''$ (equinox J2000) (Pignata et al. 2009b), which is about $17''.0$ west and $13''.5$ south of the center of the host galaxy NGC 3278. SN 2009bb was not visible in an unfiltered CHASE image ($\text{mag} < 19.2$) obtained two days prior to the discovery image on 2009 March 19.20 UT. We were therefore able to use this image in combination with the first follow-up images to obtain a tight constraint on the explosion epoch (see section 2.3).

As this was an extremely young SN, an intensive follow-up campaign was organized using the PROMPT telescopes (Reichart et al. 2005) and the facilities available to the Carnegie Supernova Project (CSP; Hamuy et al. 2006) at Las Campanas Observatory (LCO). A week after discovery, Stritzinger et al. (2009) classified SN 2009bb as a broad-lined SN Ic.

Radio and X-ray observations were obtained with the VLA and Chandra telescope. An analysis of these data indicates that SN 2009bb was associated with strong radio emission and mild X-ray emission (Soderberg et al. 2010). These findings are suggestive of the presence of a relativistic outflow typically associated with GRB-related SNe.

The explosion site of SN 2009bb has been studied in detail by Levesque et al. (2010a) who showed that contrary to other jet-driven SN explosions, which to date have always been identified with metal poor environments [see Modjaz et al. (2008) for a review], the

¹⁶Cerro Tololo Inter-American Observatory, Kitt Peak National Observatory, National Optical Astronomy Observatories, operated by the Association of Universities for Research in Astronomy, Inc., (AURA), under cooperative agreement with the National Science Foundation.

explosion site of SN 2009bb exhibits a metallicity between 1.7 to 3.5 Z_{\odot} . Levesque et al. (2010b) also found a super-solar metallicity for the environment of the long-duration GRB 020819. These findings present a challenge to the theoretical framework developed to explain GRBs (Woosley & Heger 2006). However, Dessart et al. (2008) have recently proposed a model in which the progenitor star does not need to be in a low metallicity environment. In this scenario SN 2009bb represents a peculiar object that could open new theoretical developments.

The organization of this article is as follows. The photometric data are analyzed in Section 2, and in Section 3 the pseudo-bolometric light curve is used to estimate some physical parameters of SN 2009bb. An analysis of the spectroscopic evolution of SN 2009bb is carried out in Section 4, and Section 5 presents a discussion and summary of the major results. Observation and data reduction techniques are described in Appendix A.1 and A.2.

2. Optical and Near-Infrared Photometry

2.1. Light Curve

The *BVRI* photometry of SN 2009bb is reported in Table 1, while the light curves are shown in Figure 2. Also plotted in the latter figure are photometry of the broad-lined Type Ic SNe 1998bw, 2002ap, 2003jd, 2006aj and SN 2007bg. From this comparison of light curves, it is clear that in the *VRI* bands during the pre-maximum phase, SN 2009bb, SN 2006aj and SN 2003jd show a similar evolution, while SN 1998bw and SN 2002ap have a slower and faster rise-time, respectively. In the *B* band, SN 2009bb shows, with the exception of SN 1998bw, a slower rise than all the other SNe included in the plot. At post-maximum phases (epoch $> +20$ days), the *VRI* light curves of SN 2009bb decrease in magnitude faster than the other objects, except for SN 2006aj, which appears to be quite

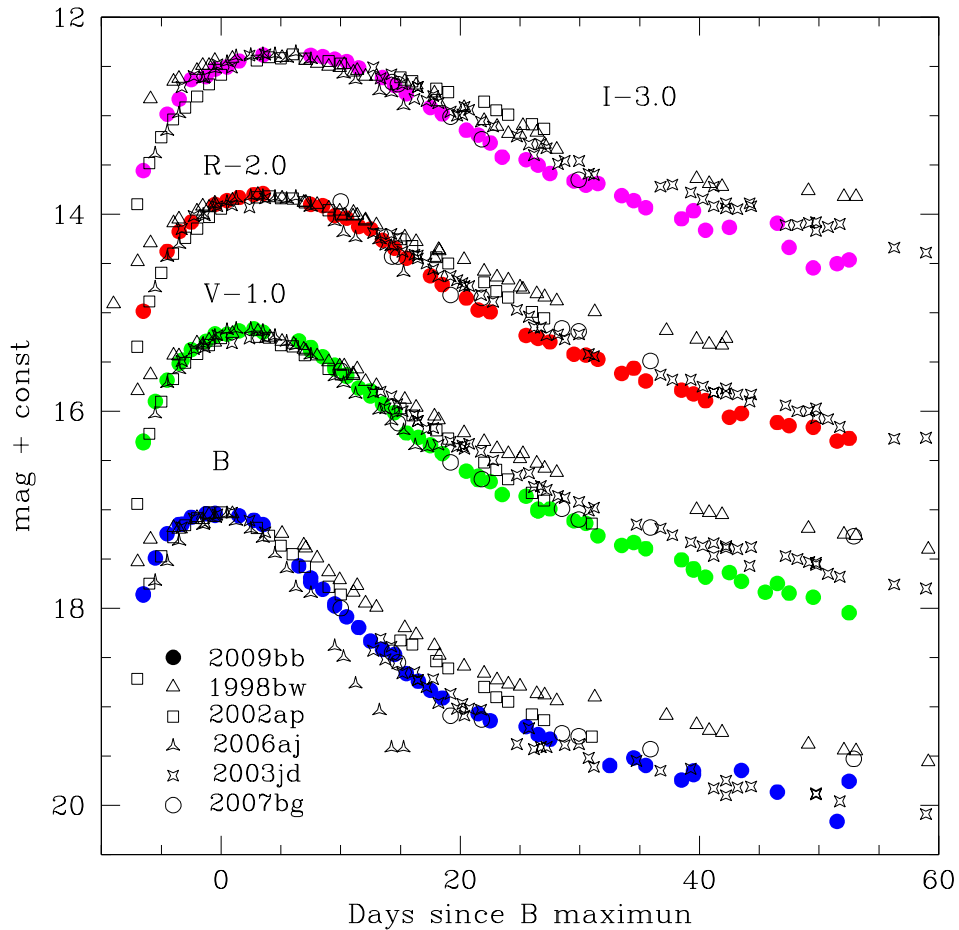


Fig. 2.— *BVRI* light curves of SN 2009bb. Our data are shown with filled circles using different colors for different filters. For comparison, the light curves of other broad-lined SNe Ic are also plotted: SN 1998bw (Galama et al. 1998; Patat et al. 2001), SN 2002ap (Foley et al. 2003), SN 2006aj (Sollerman et al. 2006; Ferrero et al. 2006), SN 2003jd (Valenti et al. 2008) and SN 2007bg (Young et al. 2010). The light curves of the different SNe were shifted to match around maximum. Different colors were shifted by different amount.

similar to SN 2009bb. This is not the case in the B band where the SN 2006aj decline rate is clearly faster than that of SN 2009bb. In the latter band, the object that most resembles SN 2009bb is SN 2003jd, while SN 2002ap and SN 1998bw display much slower decline rates.

The $u'g'r'i'z'$ photometry of SN 2009bb is reported in Table 2, while the light curves are shown in Figure 3. These are the first-ever observations of a broad-lined SN Ic in the Sloan bands. For comparison in the plot, we also include U -band light curves of SN 1998bw, SN 2002ap and SN 2006aj. The u' light curve of SN 2009bb most resembles the U -band observations of SN 2002ap, but again declines more rapidly than SN 1998bw. It should be stressed that Figure 3 compares light curves on different photometric systems, and therefore the comparison should be taken with caution.

The YJH photometry of SN 2009bb is reported in Table 3. In Figure 4, the near-infrared light curves of our SN are displayed together with those of SN 1998bw and SN 2002ap. As seen in the optical, the post-maximum evolution of SN 2009bb is slightly faster than that of SN 2002ap. In the case of SN 1998bw, the difference is larger, with the latter object being ± 0.7 and ± 0.2 magnitudes brighter than SN 2009bb in the J and H bands, respectively, at ~ 50 days past B maximum. It is worth mentioning that part of this difference could be due to host galaxy contamination affecting the SN 1998bw infrared photometry (Patat et al. 2001).

For each optical and near-infrared band, the time and value of peak magnitude was estimated from low-order polynomial fits. The results are reported in Table 4. Similar to other SNe Ib/c, maximum light occurs in the blue followed by the red bands.

In Figure 5, the count rates in the $uvw1$ and u UVOT bands at the position of SN 2009bb are plotted. The fluxes were measured in a fixed aperture and, therefore, are the sum of the light coming from the SN and the background galaxy. From the plot,

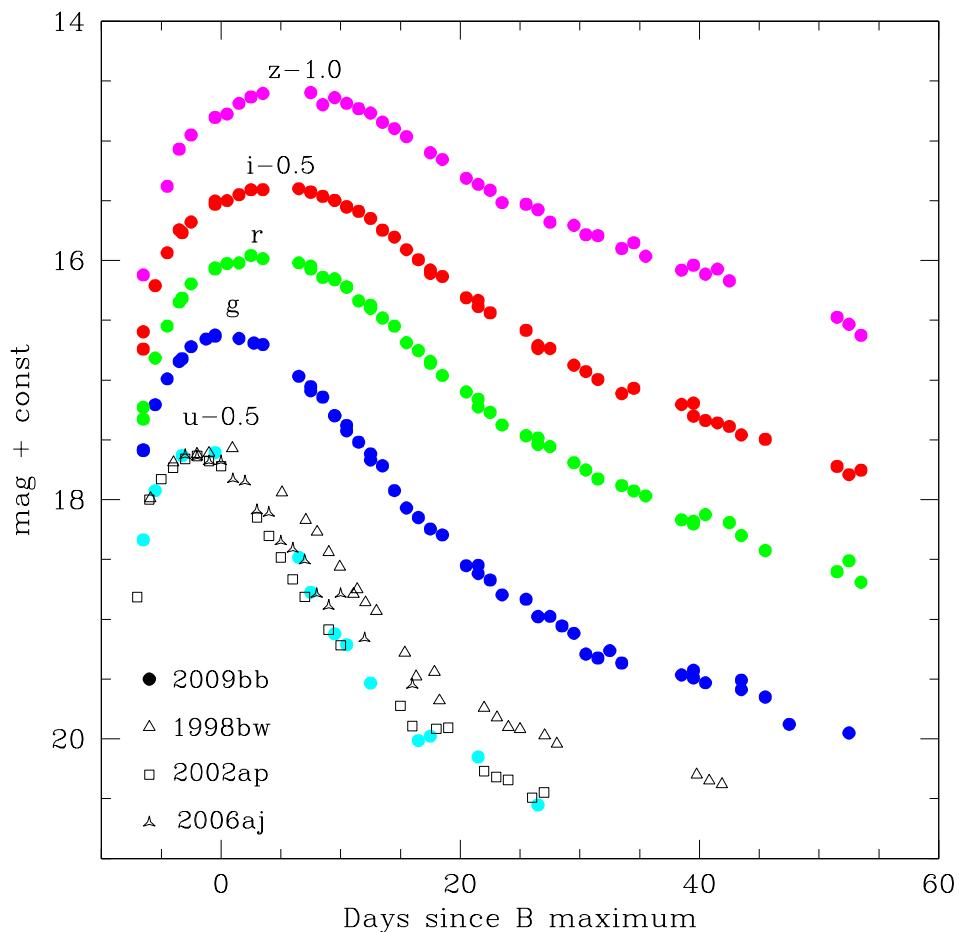


Fig. 3.— $u'g'r'i'z'$ light curves of SN 2009bb. Our data are shown with filled circles using different colors for different filters. For comparison, the U band light curves of SN 1998bw, SN 2002ap and SN 2006aj are included. The light curves of the different SNe were shifted to match around maximum. The bibliographic sources for the light curves are the same as those given in Figure 2.

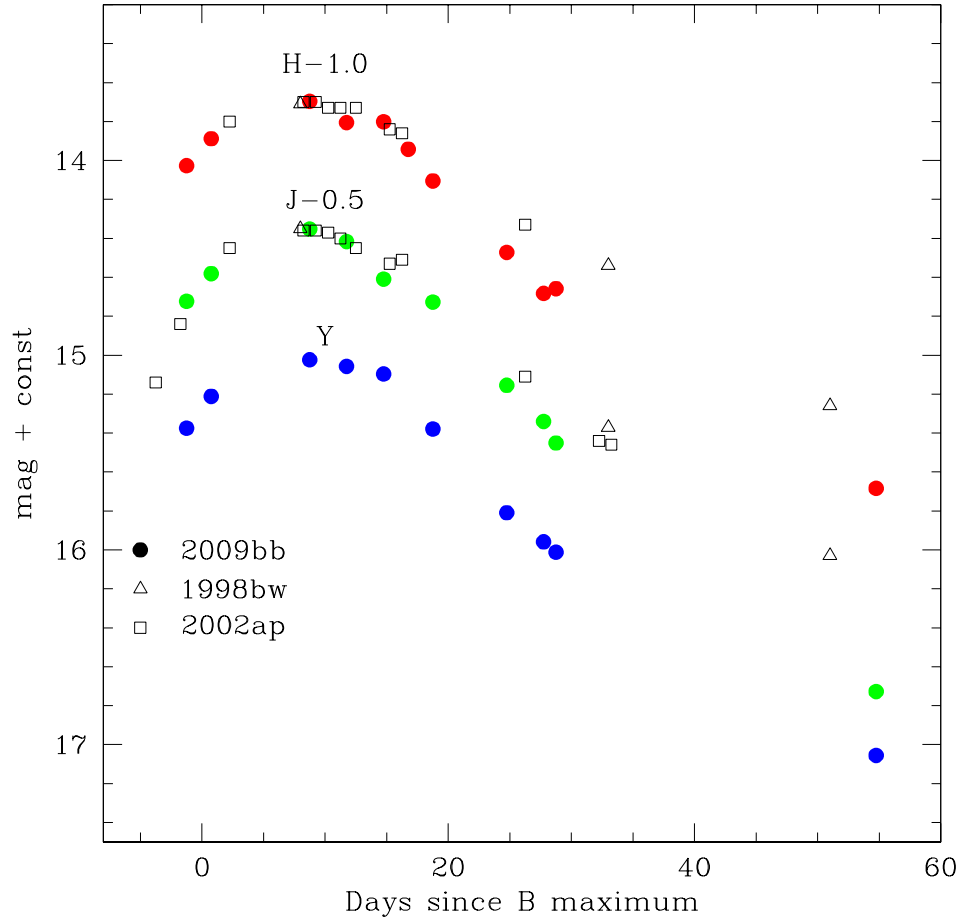


Fig. 4.— YJH light curves of SN 2009bb. Our data are shown with filled circles using different colors for different filters. For comparison, the light curves of SN 1998bw (Patat et al. 2001) and SN 2002ap (Yoshii et al. 2003) are included.

it is clear that in the *uvw1* filter, the background flux is already dominant at ~ 6 days past *B* maximum light. Assuming that the count rate measured in the last three *uvw1* observations is entirely due to the background, the SN 2009bb flux in the first observation can be estimated by subtracting the weighted average of the flux in these last three observations from the total count rate. Adding a zero point for the *uvw1* band of 17.49 ± 0.03 (Poole et al. 2008), a value of 18.1 ± 0.1 ¹⁷ is obtained for the *uvw1* magnitude of SN 2009bb at ~ 6 days before *B* maximum light.

2.2. Color Curves

The de-reddened color curves of SN 2009bb are compared in Figure 6 with those of SN 1998bw, SN 2002ap, SN 2006aj, and SN 2003jd. In the case of SN 2009bb, a color excess of $E(B - V) = 0.58 \pm 0.07$ is assumed (see Section 3), while for SN 1998bw, SN 2002ap, SN 2003jd, and SN 2006aj, values of 0.06 (Patat et al. 2001), 0.08 (Foley et al. 2003), 0.14 (Valenti et al. 2008), and 0.18 (Sollerman et al. 2006; Campana et al. 2006), respectively, were adopted. It is worth mentioning that for all the latter SNe most of the reddening is produced in the Milky Way. All the authors cited above assumed little or no reddening in the host galaxy due to the absence of strong interstellar Na I D absorption in the SNe spectra. Since the correlation between Na I D *EW* and reddening has been shown to have a significant dispersion (Folatelli et al. 2010; Olivares et al. 2010; Stritzinger et al. 2010), the reddening estimates for these SNe should be taken with caution. To convert the color excesses to corrections for each band, we adopted an R_V value of 3.1

¹⁷Additional source of uncertainties related with the red wing of the *uvw1* filter are difficult to quantify due to the lack of spectra covering the band. Therefore, they were not included in the error budget

(Cardelli, Clayton & Mathis 1989).

As is seen in Figure 6, the color evolution of broad-lined SNe Ic show significant variations. This highlights the inadequacy of color indices to estimate host galaxy extinction for these events. The early phase $(B - V)_0$ color evolution of SN 2009bb is seen to be most comparable to that of SN 2003jd, while SN 1998bw is ~ 0.2 mag redder at early and late epochs, but is similar to SN 2009bb between +10 and +20 days. In the case of $(V - R)_0$, all SNe have very similar evolution except for SN 2006aj which is ~ 0.2 redder. The $(R - I)_0$ color evolution of SN 2009bb is intermediate between SN 2002ap (bluer) and SN 2003jd (redder).

In Figure 7, we compare the reddening-corrected $(V - J)_0$ and $(V - H)_0$ color curves of SN 2009bb with those of SN 2002ap. The evolution of the two SNe is similar, but SN 2009bb is ~ 0.3 and ~ 0.5 mag bluer in $(V - J)_0$ and $(V - H)_0$, respectively.

2.3. Explosion Date

The short time interval between the CHASE images with negative and positive detection of SN 2009bb allows us to place strong constraints on its explosion date. This is done through the use of a simple equation describing an expanding fireball:

$$L(t) = K \times (t - t_0)^n, \tag{1}$$

where L is the luminosity at time, t , K is a constant that defines the rate of the rise, $n=1.8$ (Conley et al. 2006), and t_0 is the time of explosion. Applying the equation (1) to the unfiltered light curve, we estimate that the explosion occurred on $\text{JD}=2454909.6 \pm 0.6$, which corresponds to the time of our non-detection of SN 2009bb.

As demonstrated in Figure 8, the curve fits reasonably well the unfiltered light curve

(reduced $\chi^2=3.1$), except for the epoch of first detection.

3. Absolute Luminosity

To compute the absolute luminosity of SN 2009bb requires estimates of the host galaxy dust extinction and distance. One method to estimate the host reddening of SN 2009bb is to measure the Balmer decrement from the spectrum of the H II region located beneath the SN. To this end we use the two SN 2009bb nebular spectra acquired on Jan 9th and Feb 3th 2010¹⁸. In these spectra the signal-to-noise ratio of the H II region is higher than in the spectra taken at earlier epochs, while the SN flux is lower, allowing for a more precise measurement of emission from the Balmer lines. Obtaining an accurate estimate of the H_α and H_β fluxes requires the removal of the light of the SN and any residual stellar contribution. This was accomplished by fitting a cubic spline to the underlying continuum in the spectrum. The resulting pseudo-continuum was then subtracted from the original spectrum. Comparing the measured H_α/H_β flux ratio obtained from the “cleaned” spectra to the values listed in Osterbrock (1989) (for case B recombination, $T=10000^\circ$ K) and assuming the standard total-to-selective extinction ratio $R_v = 3.1$, we obtain a total reddening (host+Milky Way) of $E(B - V)_{tot} = 0.59 \pm 0.10$ and $E(B - V)_{tot} = 0.57 \pm 0.10$ for the 2010 Jan 9 and 2010 Feb 3 spectra, respectively. There is another (brighter) H II region located $\sim 0.3''$ North, $\sim 1.4''$ East of the SN. A measurement of the Balmer decrement from its spectrum gives a color excess of $E(B - V)_{tot} = 0.56 \pm 0.10$, which is in good agreement with that obtained at the SN position. Given the similarity of the three estimates, we will assume the total reddening suffered by SN 2009bb to be the average of the values obtained from its two nebular spectra, i.e. $E(B - V)_{tot} = 0.58 \pm 0.07$.

¹⁸In this spectrum there is not significant SN signal

An alternative method often used to estimate the reddening suffered along the line-of-sight to a SN is the equivalent width (EW) of the interstellar Na I D absorption. The weighted average of the EW measured from seven of our low resolution spectra is $EW = 2.16 \pm 0.12 \text{ \AA}$. Taking into account relation between the Na I D EW and color excess reported in Turatto, Benetti & Cappellaro (2003), a value of $E(B - V)_{\text{host}} = 0.34$ and $E(B - V)_{\text{host}} = 1.06$ is implied for the lower and higher slope, respectively. This confirms that SN 2009bb was significantly extinguished. Nevertheless, since the Na I D lines are almost certainly saturated, this value of $E(B - V)_{\text{host}}$ should be taken as a lower limit only. Combining the Galactic reddening obtained from the infrared dust maps of Schlegel, Finkbeiner & Davis (1998), $E(B - V)_{\text{galactic}} = 0.098$, and the host galaxy value, we obtain a lower limit of the total reddening of $E(B - V)_{\text{tot}} = 0.44$ and $E(B - V)_{\text{tot}} = 1.16$, respectively, bracketing the reddening obtained from the Balmer decrement.

Despite the relative proximity of NGC 3278, there are no direct distance measurements to this galaxy reported in the literature. We therefore must resort to the recession velocity and Hubble’s law to compute the distance to SN 2009bb. In the remainder of this paper we assume a distance modulus of $\mu = 33.01 \pm 0.15$ as given in the NASA/IPA Extragalactic Database (NED). This value is obtained from a heliocentric velocity of $2961 \pm 37 \text{ km s}^{-1}$ (Strauss et al. 1992), corrected for Virgo Infall and Great attractor (Mould et al. 2000), and assuming $H_0 = 73.0 \pm 5 \text{ km s}^{-1} \text{ Mpc}^{-1}$ (Spergel et al. 2007). Using the maximum light magnitudes reported in Table 4, and the previously mentioned values of reddening and distance, we compute absolute magnitudes for the various bands that are listed in Table 4.

Figure 9 shows the pseudo-bolometric light curve of SN 2009bb, together with SN 1998bw, SN 2002ap, SN 2003jd and SN 2006aj, obtained by integrating the absolute flux in the $BVRI$ bands. The peak luminosity of SN 2009bb is found to be close to that of SN 2006aj, and $\sim 60\%$ of that of SN 1998bw.

To estimate the ^{56}Ni content and the ejected mass, we integrated the flux of SN 2009bb contained within the $u'BVRIJH$ bands. Also included was a K band correction based on the SN 2002ap light curves (Yoshii et al. 2003). The resulting pseudo-bolometric light curve was then modeled making use of an analytical description for the peak of the light curve (Arnett 1982). The model assumes spherical symmetry, homologous expansion, no mixing of ^{56}Ni , radiation-pressure dominance, and the applicability of the diffusion approximation for photons, which restricts it to early phases (< 30 days post-explosion) when the density is sufficiently high to make the ejecta optically thick. We also assume constant opacity $k_{opt} = 0.08 \text{ cm}^2 \text{ g}^{-1}$ as computed for SN 1997ef by Mazzali et al. (2000). Chugai (2000) used a time variable opacity for modelling the SN 1998bw bolometric light curve which average value during the first 20 days after the explosion is $k_{opt} = 0.07 \text{ cm}^2 \text{ g}^{-1}$. We assume the uncertainty on visible opacity to be the difference of the previously mentioned values i.e. $0.01 \text{ cm}^2 \text{ g}^{-1}$. In Arnett (1982) model, the time-evolution of luminosity is given by

$$L(t) = M_{Ni} \epsilon_{Ni} e^{-x^2} \int_0^x 2ze^{-2xy+z^2} dz, \quad (2)$$

where ϵ_{Ni} is the energy produced in 1 second by 1 gram of ^{56}Ni , $x=t/\tau_m$ and $y=\tau_m/2\tau_{Ni}$ with τ_{Ni} being the e -folding time of the ^{56}Ni decay and τ_m effective diffusion time, which determines the width of the bolometric light curve.

If τ_m is expressed as a function of k_{opt} , the ejecta mass, M_{ej} , and the photospheric velocity, v_{ph} at time of bolometric maximum, the effective diffusion time can be written (Arnett 1982) as

$$\tau_m \sim \left(\frac{k_{opt} M_{ej}}{v_{ph}} \right)^{1/2}. \quad (3)$$

In addition to the M_{ej} and M_{Ni} parameters, there is also an additional free parameter,

T_{rise} , which is the time interval between explosion and the peak of the bolometric light curve. Finally, as proposed by Valenti et al. (2008), we include the contribution of the ^{56}Co decay in equation 2.

In this analytic model, the photospheric velocity at the time of the maximum of the bolometric light curve is an input parameter. The velocity derived from the minimum of the Si II $\lambda 6355$ feature is often used as a proxy for the photospheric velocity. Nevertheless, several studies have found that in SN Ic the Si II $\lambda 6355$ could be contaminated by other species like detached He I $\lambda 6678$, Ne I $\lambda 6402$, detached H_α or detached C II $\lambda 6580$ (Clocchiatti et al. 1996; Branch et al. 2006; Sauer et al. 2006; Elmhamdi et al. 2006). Contamination from other ions could shift the minimum of the Si II $\lambda 6355$ feature in different direction at different epochs, biasing the estimation of the photospheric velocity. In spite of these shortcomings the Si II $\lambda 6355$ feature is still the most easy feature to measure, but a correction must be applied to derive a velocity as close as possible to the real photospheric velocity at a given epoch. To compute this correction we consider SN 1998bw, SN 2002ap and SN 2006aj, for which the evolution of the photospheric velocity was computed using the Montecarlo code described in Mazzali et al. (2001). Comparing the velocities measured from the minimum of the Si II $\lambda 6355$ absorption with those derived through the spectra modelling mentioned above, a difference of $\sim 3000 \text{ km s}^{-1}$ is found. Assuming that this velocity shift also applies to SN 2009bb, we derive $v_{\text{ph}} = 15000 \pm 1000 \text{ km s}^{-1}$ at the time of the bolometric maximum light ($\text{JD}=2454923.1 \pm 0.7$). The analytical model then yields $M_{\text{Ni}} = 0.22 \pm 0.06 M_\odot$, $M_{\text{ej}} = 4.1 \pm 1.9 M_\odot$ and $T_{\text{rise}}=11.3 \pm 0.8$ days. The uncertainties in the latter quantities were computed through Montecarlo simulations, taking into account the errors in the photospheric velocity, optical opacity, distance modulus, reddening and photometry. The resulting model is compared to the computed bolometric light curve in the insert of Figure 9.

The ejecta mass and photospheric velocity allow us to estimate the kinetic energy associated with the 2009bb explosion by comparing the pseudo-bolometric light curve of SN 2009bb with that of SN 2002ap, for which detailed modelling have been already carried out (Mazzali et al. 2002). To compute the kinetic energy, equation 3 can be written as follows:

$$\tau_m \propto k_{opt}^{1/2} M_{ej}^{3/4} E_{kin}^{-1/4}. \quad (4)$$

Around maximum the pseudo-bolometric light curves of SN 2002ap and SN 2009bb are similar (see the rescaled pseudo-bolometric light curve of SN 2002ap in the insert of Figure 9). The decline rate of SN 2002ap is slightly slower than SN 2009bb. Around two weeks after B maximum, which is the latest time we considered in the bolometric light curve fit, SN 2002ap reaches the same brightness of SN 2009bb ~ 3 days later than the latter SN. Nevertheless, the rise to maximum of SN 2002ap seems to be faster than that of SN 2009bb. Computing the rise time of the bolometric light curve as difference between the explosion date and the epoch on which the bolometric light curve reach the maximum, we obtain a rise time of ~ 13.5 and ~ 10 days for SN 2009bb and SN 2002ap respectively. We therefore can assume $\tau_{m_{2009bb}} \sim \tau_{m_{2009ap}}$. Taking into account that for SN 2002ap $M_{ej} = 2.5 \pm 0.5 M_{\odot}$ and $E_{kin} = 4 \pm 1 \times 10^{51}$ erg (Mazzali et al. 2007), for SN 2009bb we obtain $E_{kin} = 1.8 \pm 0.7 \times 10^{52}$ erg.

4. Evidence for a Central Engine

Radio observations of SN 2009bb spanning $\Delta t \approx 17 - 100$ days after the explosion revealed evidence for an extraordinarily luminous, long-wavelength counterpart, with a spectral luminosity L_{ν} at $\nu = 4.9$ GHz of $\approx 5 \times 10^{28}$ erg s $^{-1}$ (Soderberg et al. 2010). In

comparison to the other ~ 150 nearby SNe Ibc observed in the radio on a similar timescale, SN 2009bb is a factor of 10 to 10^3 more luminous, rivaling the radio afterglow luminosities of the nearest GRB-SNe, including GRB 980425 associated with SN 1998bw (Kulkarni et al. 1998). The multi-frequency radio observations were well described by a self-absorbed synchrotron spectrum, produced as the blast-wave shock-accelerated electrons in the local circumstellar medium. Just as in the case of SN 1998bw, the high brightness temperature of the SN 2009bb radio counterpart required an unusually large emitting region and, in turn, a trans-relativistic blast-wave velocity, $v \approx 0.9c$. Moreover, the high radio luminosity implied a copious energy coupled to the fastest ejecta, $E \gtrsim 10^{49}$ erg. Soderberg et al. (2010) appealed to a model where this trans-relativistic ejecta component was powered by a different mechanism, a “central engine” (rapidly-rotating and accreting black hole or magnetar), as is commonly assumed for long-duration GRBs (MacFadyen, Woosley & Heger 2001).

This model can be tested using the bulk explosion parameters (E_K , M_{ej}) for SN 2009bb derived from our well-sampled optical photometry and spectroscopy. Analytic solutions for the distribution of ejecta in Type Ibc SNe predict a steep coupling of energy and velocity within the homologously-expanding material,

$$E(v) \approx 3.7 \times 10^{47} \left(\frac{E_{\text{SN}}}{10^{51}} \right)^{3.59} \left(\frac{M_{\text{ej}}}{M_{\odot}} \right)^{-2.59} \left(\frac{v}{0.1c} \right)^{-5.18} \text{ erg} \quad (5)$$

(Matzner & McKee 1999; Berger, Kulkarni & Chevalier 2002). Based on an analysis of the optical dataset (see Section 3), we find bulk ejecta parameters of $E_K \approx 1.8 \times 10^{52}$ erg and $M_{\text{ej}} \approx 4.1 M_{\odot}$. Within the homologous outflow, we therefore expect the ejecta traveling at $v \gtrsim 0.9c$ to carry a kinetic energy of $E_K \approx 3.5 \times 10^{45}$ erg. This is *at least* three orders of magnitude below the energy budget required to power the trans-relativistic radio emitting ejecta. We conclude that the luminous synchrotron emission from SN 2009bb cannot be

explained in the framework of a homologous SN explosion and another energy reservoir (i.e. a central engine) is required to explain the distribution of ejecta within this relativistic SN.

5. Spectroscopy

Optical spectra of SN 2009bb were obtained on thirteen epochs spanning phases between -2 and $+285$ days. Table 5 provides a log of these observations, and Figure 10 illustrates the spectral evolution.

5.1. General evolution

Comparing the de-reddened spectra of SN 2009bb to similar epoch spectra of SN 1998bw, SN 1997ef, SN 2003jd and SN 2002ap, de-reddened using the color excess values mentioned in Section 3, one can note that at early phases SN 2009bb, SN 2003jd and SN 2006aj are characterized by a bluer continuum than SN 1997ef and SN 2002ap (see Figures 11 and 12). Around two week past maximum, the continuum has become similar to that of all the other comparison SNe.

In terms of degree of broadening of the spectral features around maximum, the spectra of SN 2009bb are similar to those of SN 2006aj (see Figure 11 and 12). Looking at the SN 2009bb spectra taken later than a week after B maximum (see Figure 13, Figure 14 and 15), the degree of blending is still high in SN 2009bb being intermediate between SN 2003jd and SN 1998bw. This slow spectroscopic evolution in spite of the high expansion velocity is a further indication that SN 2009bb had a massive envelope. The expansion velocity of 2009bb decreases similarly to that of SN 1998bw and slower SN 2002ap (see Figure 16).

5.2. Detailed Comparison: the Helium Detection

In the following, the evolution of some features present in the spectra of SN 2009bb are analyzed in more detail using the supernova spectrum-synthesis code SYNOW (Jeffery & Branch 1990; Branch, Baron, & Jeffery 2003). Particular effort is devoted to determining if helium is present in the ejecta of SN 2009bb, as this is very important for constraining the nature of its progenitor and its evolutionary stage at the time of the explosion. We explore qualitatively the presence of helium using SYNOW, but it must be kept in mind that full spectral modeling, including non-thermal effects is necessary to study quantitatively the evolution and strength of the He lines (Lucy 1991).

The clearest evidence of the presence of helium in the SN 2009bb ejecta is found in the first two spectra taken at -2 and -1 days (see Figure 11). A striking feature in these two spectra is the absorption around 5400 \AA . This line is not visible in the other SNe spectra, and we suggest that it corresponds to He I $\lambda 5876$. Fitting the line profile with SYNOW, we obtain a good match for a velocity in the line forming region of $\sim 28000 \text{ km s}^{-1}$ and 27500 km s^{-1} in the -2 and -1 days spectra, respectively. A similar velocity is also obtained by fitting the absorption around 4800 \AA with Fe II $\lambda\lambda 4924, 5018, 5169$ and also provides a good match with Si II $\lambda 6355$ for the absorption located at $\sim 5800 \text{ \AA}$. In Figure 11, the expected positions of the He I $\lambda 6678$ and He I $\lambda 7065$ absorption are also marked. In both the -2 and -1 day spectra, features are present at this wavelength, but due to their weakness and to strong background contamination, should not be over-interpreted.

In Figure 12 we show the SN 2009bb spectrum taken at $+4$ days. The velocity obtained from SYNOW fits to Fe II $\lambda\lambda 4924, 5018, 5169$ and Si II $\lambda 6355$ is $\sim 18000 \text{ km s}^{-1}$. SN 2009bb shows the closest resemblance to SN 2006aj, but differences are visible particularly around the Si II $\lambda 6355$ absorption and between 5000 and 6000 \AA , where SN 2009bb clearly differs compared to the other SNe. Attributing this absorption to detached He I at $\sim 25000 \text{ km s}^{-1}$,

we obtain a reasonable fit of the observed feature (see short dashed green line in Figure 17).

The expected positions of the other He I features for the assumed detached velocity ($\sim 25000 \text{ km s}^{-1}$) are indicated in Figure 12. Indeed, an absorption corresponding to He I $\lambda 6678$ appears to be present and helps to fit the boxy profile of the Si II line (see Figure 17). There is also a weak feature corresponding to the expected position of He I $\lambda 7065$, but contamination from Ne I $\lambda 6929$ cannot be excluded.

Figure 13 shows the spectrum of SN 2009bb taken a week after B -band maximum. Between 5000 and 5500 \AA , SN 2002ap and SN 2003jd show an absorption apparently due to Na I. This feature is absent in the spectra of SN 2009bb, SN 1998bw and SN 1997ef, which is probably due to the broadness of the spectral features in the latter SNe, that tends to wash out weak features. Nonetheless, the absence of a clear feature in the SN 2009bb makes less plausible the possibility that in the earlier SN 2009bb spectra the absorption around 5500 \AA is due to Na I. As shown in Figure 17, He I with a detached velocity of $\sim 23000 \text{ km s}^{-1}$ gives a good fit to the observed line profile between 5000 and 5500 \AA . Figure 13 also shows the spectrum of the broad lined Type Ic SN 2007bg, for which the He I lines (the positions of the He I $\lambda 7065$, $\lambda 7235$ lines are marked in the graph) appear to be even stronger than observed in the spectrum of SN 2009bb. Unfortunately, due to the higher expansion velocity of the absorption features in SN 2009bb, the He I $\lambda 7065$ line falls in the gap between the CCDs, making its presence impossible to confirm.

Figure 14 shows a spectrum of SN 2009bb taken two weeks after B -band maximum. The absorption feature around 5500 \AA is still deeper in SN 2009bb than in the other two SNe. For SN 2009bb, an equally good fit to this feature is obtained with Na I undetached ($\sim 14000 \text{ km s}^{-1}$), or with He I $\lambda 5876$ detached at $\sim 18000 \text{ km s}^{-1}$. Again, the expected positions of the other prominent He I lines are indicated in this Figure, but clear signs of these features cannot be seen in the SN 2009bb spectrum.

Figure 15 displays the spectra taken on days +30 and +44. The emission redward of the Na I absorption remains stronger in SN 2009bb compared to the other SNe plotted in this Figure, but the profile around the Na I absorption is now not so different suggesting a reduced strength of the blue wing of the He I $\lambda 5876$ detached component. In both the +33 and +44 spectra of SN 2009bb, there also is no clear signature of the He I $\lambda 6678$ and $\lambda 7065$ features. It should be noted that in the rather noisy spectrum of SN 2007bg, the helium lines, if present, are not as strong as expected. In the case of helium-rich core-collapse SNe (SNe Ib), the He I features are stronger at these later epochs than at maximum (e.g. Matheson et al. 2001). A possible explanation for the lack of strengthening of the He I absorption features in the case of SN 2009bb (and perhaps also for SN 2007bg) is that, due to the higher expansion velocity of broad-lined SNe Ic together with a less massive helium shell, the mass of helium in the line forming region at these later epochs is likely much lower than in normal SNe Ib.

The evolution of the He I $\lambda 5876$ velocity is summarized in the insert of Figure 16. Before maximum He is undetached from the main line forming region, while after maximum is detached. This agrees with the finding of Branch et al. (2002) and Elmhamdi et al. (2006) for Type Ib SNe. The velocity of the detached He decrease with time. The latter also agree with what obtained by Branch et al. (2002).

The fractional line depth of the O I $\lambda 7774$ line can, in principle, be used to infer the presence of helium using the formula given by Matheson et al. (2001)

$$\text{Fractional line depth} = \frac{F_{cont} - F_{min}}{F_{cont}}, \quad (6)$$

where F_{cont} and F_{min} represent the values of the continuum and of the line minimum at the wavelength of the minimum, respectively. The latter authors proposed that in SNe Ib, due to the dilution of oxygen by helium, the O I $\lambda 7774$ absorption should be weaker than

in SNe Ic. Indeed, they measured an average fractional line depth of 0.27 ± 0.11 and 0.38 ± 0.09 for SNe Ib and SNe Ic, respectively. Matheson et al. (2001) also found that this difference is stronger around maximum than at late time. Unfortunately, in broad-lined SNe Ic, the depth of the O I $\lambda 7774 \text{ \AA}$ is difficult to measure at early epochs due to the widths of the other lines in this spectral region. In Figure 18, measurements at phases later than +20 days are plotted. As for normal SN Ibc the fractional line depth for broad-lined SNe Ic increases with time. Interestingly, the two broad-lined SNe Ic which show evidence of helium lines, SN 2009bb and SN 2007bg, have an O I $\lambda 7774$ line depth that is less than those that do not show any sign of helium. Note that Figure 18 does not include SN 1998bw since, even at +50 days, O I $\lambda 7774$ is still strongly blended with the Ca II near-infrared triplet.

5.3. Nebular Spectrum

In Figure 19 we show a comparison between the nebular spectra of SN 2009bb, SN 1997ef, SN 1998bw, SN 2002ap and SN 2006aj. To study the line profiles of SN 2009bb, the strong emission lines from the underlying H II region must be removed. This was achieved by subtracting the spectrum of the bright H II region located $\sim 0.3''$ North, $\sim 1.4''$ East of the SN position. The latter spectrum was acquired with the same spectrograph, making more accurate the spectra matching procedure. The spectrum of the bright H II region was rescaled to match the line fluxes of the H II region underlying the SN. Note that the line ratios for the two H II regions are similar to within 10%. This, together with the very similar Balmer decrement measured in the two H II regions (see section 3), gives confidence that the subtraction procedure has not significantly altered the SN spectrum.

The nebular spectrum of SN 2009bb is rather noisy, but several strong emission features can be recognized. The emission in the blue, near 4500\AA , should be dominated by [Mg I]

$\lambda 4570$. The broad complex near 5200\AA is the result of a number of [Fe II] emission lines. Near 5900\AA , Na I D emission is possibly detected. The two strongest lines in the spectrum are [O I] $\lambda\lambda 6300, 6363$ and Ca II] $\lambda\lambda 7291, 7324$.

It is immediately clear that the calcium to oxygen ratio is much larger in SN 2009bb than in all the other comparison SNe. It is also evident, when compared to the spectra of SNe 2003jd and 1998bw, that the profile of the [O I] $\lambda\lambda 6300, 6354$ emission in SN 2009bb is more similar to that of SN 1998bw than that of SN 2003jd (see Figure 20). Based on spectral modelling, Mazzali et al. (2005) claimed that a double peaked [O I] $\lambda\lambda 6300, 6354$ profile as observed in SN 2003jd is produced by an aspherical expansion, but viewed off axis. Assuming that this interpretation is correct [but see also Maeda et al. (2008); Maurer et al. (2010)], in the case of SN 2009bb, the material ejected must have been oriented close to the line of sight as in the case of SN 1998bw.

The nebular spectrum of SN 2009bb can be modelled in order to derive some physical properties of the SN. Nebular spectroscopy reveals the conditions of the innermost part of the SN ejecta, which are not visible when the SN is bright because they lie too deep in regions that are optically thick. At late phases, on the other hand, the inner parts of the SN are transparent, and behave like a nebula.

The code we used computes the energy deposition from the decay of ^{56}Ni to ^{56}Co to ^{56}Fe . These decays emit γ -rays and high-energy positrons, which can deposit their energy in the SN ejecta and heat the gas by collision excitation. Cooling then takes place via line emission. Our code was described by Mazzali et al. (2001), and is based on the description of Axelrod (1980).

We model the spectrum of SN 2009bb using the simple, one-zone version of the nebular code. This assumes that the SN ejecta are spherical, and bound by an outer velocity, which reflects not so much the extent of the ejecta in radius or velocity (the two are

equivalent in the homologously expanding SN ejecta), but rather that of the region which is effectively heated and can therefore emit lines. This may be the result of decreasing density, distribution of ^{56}Ni , or both.

Our model requires an outer velocity of 5500 km s^{-1} . This velocity appears to be adequate to fit all lines. This could be taken as an argument that SN 2009bb was not significantly aspherical. In models where more energy is released in a polar direction, leading to the synthesis of ^{56}Ni and possibly to the production of a GRB, the [Fe II] lines are broader than the [O I] line if the event is viewed close to the polar axis (Maeda et al. 2003). Otherwise, the [Fe II] lines are narrower than the [O I] line, which shows a characteristic double-peaked profile, as in SN 2003jd. Nevertheless, the strongest evidence for asphericity in SN 1998bw was seen in nebular spectra obtained 200 days after maximum (Mazzali et al. 2001), while the difference between the iron and oxygen lines width was smaller at epochs of 340 days, which is closer to the epoch of the only nebular spectrum available for SN 2009bb. Therefore, while from this spectrum only we do not infer major asphericities in SN 2009bb, we cannot rule out that the signature of asphericity might have been seen in earlier nebular data.

The ^{56}Ni mass which is required to reproduce the spectrum, assuming a distance modulus of 33.0 and a reddening $E(B - V) = 0.58$, is $0.25 M_{\odot}$. This is in good agreement with the estimate of $0.22 \pm 0.06 M_{\odot}$ found from modelling the pseudo-bolometric light curve. The mass of the elements used to generate the synthetic spectra are summarized in Table 6.

6. Discussion and conclusions

We have presented UV, optical and near-infrared photometry, and optical spectroscopy of the broad-lined Type Ic SN 2009bb. Around maximum, the spectra of SN 2009bb were

similar to those of SN 2003jd and SN 2006aj. The expansion velocities of SN 2009bb are similar to these of SN 2006aj, but higher than those of SN 2003jd. At phases later than +15 days, the broadness of the spectral features in SN 2009bb was intermediate between SN 1997ef and SN 1998bw. The slow spectroscopic evolution indicates that SN 2009bb had a massive envelope, and this is confirmed by the pseudo-bolometric light curve analysis. With a simple model that includes both the ^{56}Ni and ^{56}Co decay, and making use of analytic equations presented in Arnett (1982), we obtain a ^{56}Ni and ejected mass of $0.22 \pm 0.06 M_{\odot}$ and $4.1 \pm 1.9 M_{\odot}$, respectively. The resulting kinetic energy is 18 ± 7 Foe. A similar ^{56}Ni mass is obtained from the nebular spectrum modelling $M_{^{56}\text{Ni}} = 0.25 M_{\odot}$.

An absorption feature is identified in the -2 and -1 day spectra around 5400 \AA that we attribute to He I $\lambda 5876$ forming at the photosphere. He I appears to be detached in the later spectra, with the absorption getting weaker with time. The latter evolution is odd compared to what is normally observed in SNe Ib where helium lines become stronger after maximum. The weakening of the helium absorption could be due to a combination of the fast expansion characteristic of broad-lined SNe and a less massive helium shell than in “normal” SN Ib.

The comparison between the kinetic energy carried away by the homologous expanding ejecta at $v \gtrsim 0.9c$ and the energy inferred by the radio observations points to the need for an extra source of energy provided by a central engine.

The modelling of the SN 2009bb nebular spectrum indicates that iron and oxygen lines can be reproduced with a synthetic spectrum where both elements have similar expansion velocities. This suggests that SN 2009bb ejecta structure was not significantly aspherical. Nonetheless, considering the iron and oxygen lines evolution of SN 1998bw, we cannot exclude that the signature of asphericity could have been detected in a SN 2009bb earlier nebular spectrum. The analysis of the [O I] $\lambda\lambda 6300, 6354$ reveals that, if the explosion was

indeed aspherical, the orientation should have been similar to that of SN 1998bw. Therefore, if a GRB was produced during the SN2009bb explosion, it was below the threshold of the current generation of γ -ray instruments. Without a detected GRB counterpart, SN 2009bb represents the first engine-driven, relativistic supernova ever discovered by its optical emission alone. The presence of a relatively massive helium layer may have played a role on the failed GRB detection, but a quantitative description of the helium shell is necessary to verify this hypothesis.

A special thanks to the Gemini-South staff for their efforts in obtaining data for our spectroscopic program. G.P. acknowledges support by the Proyecto FONDECYT 11090421 and from Comité Mixto ESO-Gobierno de Chile. M.H. acknowledges support from FONDECYT through grant 1060808. G.P., M.H. and J.M. acknowledge support from the Millennium Center for Supernova Science through grant P06-045-F funded by “Programa Bicentenario de Ciencia y Tecnología de CONICYT”, “Programa Iniciativa Científica Milenio de MIDEPLAN”. G.P., M.H. and J.M. acknowledge partial support from Centro de Astrofísica FONDAF 15010003 and by Fondecyt through grant 1060808 from the Center of Excellence in Astrophysics and Associated Technologies (PFB 06). The Dark Cosmology Centre is funded by the Danish NSF. This material is based upon work supported by the National Science Foundation (NSF) under grant AST-0306969. This paper is based on observations obtained at the Gemini Observatory, Cerro Pachon, Chile (Gemini Programs GS-2009A-Q-17 and GS-2009A-Q-43). We have made use of the NASA/IPAC Extragalactic Database (NED) which is operated by the Jet Propulsion Laboratory, California Institute of Technology, under contract with the National Aeronautics and Space Administration.

A. Observations and data reduction

Imaging of SN 2009bb was acquired with five different instruments in the optical, one in the near-infrared, and one in the ultraviolet. A summary of the characteristics of the facilities used are listed below.

A.1. Photometry

- The SWIFT space telescope is equipped with the UVOT camera that has 256×256 physical pixels, but after processing the final combined images has 2048×2048 pixels with a pixel scale of $0''.5$. SN 2009bb was observed with the *uvw1* and *u* filters.
- The PROMPT 3 telescope at CTIO is equipped with a CCD camera Alta U47UV E2V CCD47-10 (1024×1024 , pixel scale = $0''.6$ per pixel). SN 2009bb was observed with both a standard Johnson-Kron-Cousins *B*-band and a Sloan *g'* filters.
- PROMPT 5 is equipped with a CCD camera Alta U47 E2V CCD47-10 (1024×1024 , pixel scale = $0''.6$ per pixel). SN 2009bb was observed with both Johnson-Kron-Cousins *VRI* and Sloan *r'i'z'* filters.
- The 1.0 m Henrietta Swope telescope at LCO is equipped with a SITe3 CCD camera (2048×3150 , pixel scale = $0''.435$ per pixel). SN 2009bb was observed with both Johnson-Kron-Cousins *BV* and Sloan *u'g'r'i'* filters.
- The Swope telescope was also used to obtain near-infrared *YJH* imaging with the RetroCam camera (HAWAII-1 1024×1024 , pixel scale = $0''.54$)

All optical images were reduced following standard procedures including bias, dark (when appropriate), and flat-field corrections. Photometry of the supernova was computed

relative to a local photometric sequence in the field of NGC 3278. The photometric sequence itself was calibrated to the standard Johnson Kron-Cousins and Sloan photometric systems using observations of Landolt (1992) and Smith et al. (2006) photometric standard stars obtained over the course of seven photometric nights. Our adopted $BVRI$ and $u'g'r'i'z'$ photometry of the local sequence is reported in Table 7 and Table 8, respectively. The listed values were computed via a weighted average of the measurements made for each of the seven calibration nights.

Given that the background of SN 2009bb was quite complex due to the presence of a bright H II region, it was necessary to apply template subtractions to all of the optical images. Three template images for each filter were acquired with the PROMPT telescopes between 2010 May 25–30, or ~ 420 days after B maximum brightness. To estimate the SN residual flux in these templates, we rescaled the $BVRI$ light curves of SN 1998bw in order to obtain the best match with SN 2009bb between +30 and +50 days. The brightness decline of SN 1998bw is slower than that of SN 2009bb (see Figure 2), therefore a rescaling computed around maximum light should grossly overestimate the late-time flux of SN 2009bb. Interpolating the rescaled light curves at the epoch on which the SN 2009bb templates were acquired, we estimate the SN 2009bb brightness to be: $B \sim 24.6$ mag, $V \sim 24.3$ mag, $R \sim 23.3$ mag and $I \sim 23.1$ mag. Assuming zero flux in the templates, these values imply an underestimation of the SN 2009bb real flux in all the bands of less than 0.5% around maximum, and less than 2% on the last measurement published in this paper. These values make us confident that the analysis reported here is not affected by systematic errors related to template subtraction. Using the SN 2009bb spectra acquired on 2010 Jan. 9 UT and the standard bands of the Johnson-Kron-Cousins and Sloan photometric systems, we can estimate the previously mentioned systematic errors also for the $g'r'i'z'$ PROMPT light curves. As expected, also in this case the flux underestimation turns out to be negligible. Taking into account that the decline rate of SN 1998bw is slower than

SN 2009bb the previously reported SN 2009bb late phase magnitudes should be regarded as an upper limit of its real brightness. Nevertheless, possible late time flattening on the light curve cannot be excluded a priori. In order to obtain a direct estimate of the SN 2009bb residual flux in the template images, we examined the IMACS $g'r'i'$ images taken on 28 Dec. 2009 UT. We measured the flux in an aperture centered in the SN position and of a radius equal to 3 times the sigma of the Gaussian profile of the stellar objects present in the image. Through these measurements, we estimate upper limits of 20.9 mag, 20.5 mag and 20.1 mag for the $g'r'i'$ filters respectively. We note that most of the flux measured in the IMACS images is due to the galaxy emission, not from the SN itself. To prove this, we computed synthetic magnitudes on the SN 2009bb nebular spectrum acquired on 9 Jan. 2010 UT once this was cleaned from the H II region and stellar emissions. We obtained: $B=24.0$, $V=23.9$, $R=23.0$, $I=23.1$, $g'=23.84$, $r'=23.4$, $i'=23.4$ and $z'=23.8$ mag.

In the case of the Swope telescope, the template images were acquired on 20 Nov 2009 UT. The SN flux in the u' and B bands, was negligible, but this was not the case in the $Vg'r'i'$ images. In order to reliably calibrate the magnitudes in the light curve tail, we estimated the residual flux in the template images matching the PROMPT and Swope light curves around maximum.

We next proceeded to compute $BVRIg'r'i'$ photometry of SN 2009bb in the standard Johnson and Sloan systems using the S-correction technique (Stritzinger et al. 2002), but following the prescription of Pignata et al. (2008). Since the u' band is not fully covered by any of our SN 2009bb spectra, the SN magnitudes were calibrated in the standard photometric system using the following equation:

$$u' = u + 0.044 \times (u' - g') + ZP_{u'} \tag{A1}$$

where u' is the magnitude in the standard photometric system and u is the magnitude in the instrumental one, while ZP refers to the photometric zero point.

The near-infrared images were obtained using a standard jitter technique. To reduce the data cubes, we made use of a pipeline developed by the CSP (for details see Contreras et al. 2010). The pipeline applies to each image dark, flat-field, and detector linearity corrections. These altered images are geometrically aligned and then stacked to obtain a master image from which photometry was computed.

Near-infrared photometry of the SN was also obtained relative to a local sequence of stars calibrated against Persson et al. (1998) standard stars obtained during three photometric nights. The YJH photometry of the local sequence stars are reported in Table 9. Comparing our J and H magnitudes with these of the 2MASS catalog, we obtain a difference of 0.03 ± 0.03 mag and 0.02 ± 0.05 mag, respectively.

The near-infrared photometry instrumental magnitudes were computed through the template subtraction technique. As the photometry of the SN is computed differentially with respect to the local sequence, we obtained final magnitudes using the following equations:

$$Y = y + ZP_Y \tag{A2}$$

$$J = j + ZP_J \tag{A3}$$

$$H = h + ZP_H. \tag{A4}$$

Here YJH are the magnitudes in the standard photometric system, yjh are the magnitudes in the natural photometric system and ZP_Y , ZP_j , ZP_h are the zero points.

The UVOT images were reduced using the customized instrument pipeline that, in addition to preparing the frames for photometry, computes an astrometric solution for them. Aperture photometry was performed on the RA, DEC position of SN 2009bb with the optimum aperture radius of $10''$ suggested by Poole et al. (2008). To ensure that the aperture includes a constant amount of light, the stability of the PSF size was checked in all the combined images. The *r.m.s.* of the FWHM variation was 0.2 pixels for both the *uvw1* and *u* UVOT filters.

A.2. Spectroscopy

Optical spectroscopy of SN 2009bb was obtained on thirteen epochs with the du Pont (+ WFCCD & B&C) and Magellan (+IMACS & LDSS3) telescopes at LCO, and the Gemini South (+ GMOS) telescope. Spectra were reduced in a standard manner using IRAF scripts based on tasks contained within the IRAF `noao.twodspec` and `gemini.gmos` packages. Optimal extraction was obtained by weighting the signal according to the intensity profile along the slit. Sky subtraction was generally carried out by fitting a low order polynomial to both sides of the extracted SN spectrum, and wavelength solutions were determined from exposures of arc lamps. The wavelength calibration was checked against bright night-sky emission lines. Flux calibration was performed by means of spectrophotometric standard stars (Hamuy et al. 1992, 1994) and checked against the photometry. When discrepancies occurred, the flux of the spectrum was scaled to match the broad-band photometry.

REFERENCES

- Arnett W. D. 1982, ApJ, 253, 785
- Axelrod, T. S. PhD Thesis 1980
- Berger E., Kulkarni S. R., Chevalier R. A., 2002, ApJ, 577, L5
- Branch D., et al. 2002, ApJ, 566, 1005
- Branch D., Baron E. & Jeffery D. J. 2003, in Supernovae and Gamma-Ray Bursters, ed. K. Weiler (Heidelberg: Springer), 47
- Branch D., Jeffery D. J., Young T. R., Baron E., 2006, PASP, 118, 791
- Campana S., et al. 2006, Nature, 442, 1008
- Cardelli J. A., Clayton G. C., Mathis J. S., 1989, ApJ, 345, 245
- Chugai N. N., 2000, Astronomy Letters, 26, 797
- Clocchiatti A., et al. 1996, ApJ, 462, 462
- Conley A., et al. 2006, AJ, 132, 1707
- Contreras C., et al. 2010, AJ, 139, 519
- Dessart L., Burrows A., Livne E., Ott C. D. 2008, ApJ, 673, L43
- Elmhamdi A., et al. 2006, A&A, 450, 305
- Ferrero P., et al. 2006, A&A, 457, 857
- Folatelli G., et al. 2010, AJ, 139, 120
- Foley R. J., et al. 2003, PASP, 115, 1220

Galama T. J., et al. 1998, *Nature*, 395, 670

Gal-Yam A., Ofek E. O. & Shemmer O., 2002, *MNRAS*, 332, L73

Gal-Yam A., et al. 2004, *ApJ*, 609, L59

Hamuy M., Walker A. R., Suntzeff N. B., Gigoux P., Heathcote S. R., Phillips M. M., 1992, *PASP*, 104, 533

Hamuy M., Suntzeff N. B., Heathcote S. R., Walker A. R., Gigoux P., Phillips M. M., 1994, *PASP*, 106, 566

Hamuy M., et al. 2006, *PASP*, 118, 839

Hamuy M., et al. 2009, *ApJ*, 703, 1612

Hjorth J., et al. 2003, *Nature*, 423, 847

Jeffery D. J. & Branch, D. 1990, in *Supernovae*, eds. J. C. Wheeler, T. Piran, & S. Weinberg (Singapore: World Scientific). 149

Kocevski D., et al. 2007, *ApJ*, 663, 1180

Kulkarni S. R., et al. 1998, *Nature*, 395, 663

Landolt A. U., 1992, *AJ*, 104, 340

Levesque E. M., et al. 2010a, *ApJ*, 709, L26

Levesque E. M., et al. 2010b, *ApJ*, 712, L26

Lucy L. B., 1991, *ApJ*, 383, 308

MacFadyen A. I., Woosley S. E., Heger A., 2001, *ApJ*, 550, 410

Maeda K., et al. 2003, *ApJ*, 593, 931

- Maeda K., et al. 2008, *Science*, 319, Issue, 1220
- Malesani D., et al. 2004, *ApJ*, 609, L5
- Matheson T., et al. 2001, *AJ*, 121, 1648
- Matheson T., et al. 2003, *AJ*, 599, 394
- Matzner C. D., & McKee C. F. 1999, *ApJ*, 510, 379
- Maurer J. I., et al. 2010, *MNRAS*, 402, 161
- Mazzali P. A., et al. 2000, *ApJ*, 545, 407
- Mazzali P. A., et al. 2001, *ApJ*, 559, 1047
- Mazzali P. A., et al. 2002, *ApJ*, 572, L61
- Mazzali P. A., et al. 2005, *Science* 308, 1284
- Mazzali P. A., et al. 2007, *ApJ*, 670, 592
- Modjaz M., et al. 2006, *ApJ*, 645, L21
- Modjaz M., et al. 2008, *AJ*, 135, 1136
- Mould J. R., et al. 2000, *ApJ*, 529, 786
- Olivares F., et al. 2010, *ApJ*, 715, 833
- Osterbrock D. 1989, *Astrophysics of gaseous nebulae and active galactic nuclei* (University Science Books)
- Patat F., et al. 2001, *ApJ*, 555, 900
- Persson S. E., Murphy D. C., Krzeminski W., Roth M., Rieke M. J., 1998, *AJ*, 116, 2475

Pian E., et al. 2006, *Nature*, 442, 1011

Pignata G., et al. 2008, *MNRAS*, 388, 971

Pignata G., et al. 2009a, in the proceeding of Probing stellar populations out to the distant universe. AIP Conference Proceedings, Volume 1111, pp. 551

Pignata G., et al. 2009b, *CBET* 1731

Poole T. S., et al. 2008, *MNRAS*, 383, 627

Reichart D., et al. 2005, *Il Nuovo Cimento C*, 28, 767

Sahu D. K., et al. 2009, *ApJ*, 697, 676

Sauer D., et al. 2006, *MNRAS*, 369, 1939

Schlegel D. J., Finkbeiner D. P., Davis M., 1998, *ApJ*, 500, 525

Smith J. A., et al. 2006, *AJ*, 123, 2121

Soderberg A. M., et al. 2010, *Nature*, 463, 513

Sollerman J., et al. 2006, *A&A*, 454, 503

Spergel D. N., et al. 2007, *ApJS*, 170, 377

Stanek K. Z., et al. 2003, *ApJ*, 591, L17

Strauss M. A., et al. 1992, *ApJS*, 83, 29

Stritzinger M., et al. 2002, *AJ*, 124, 2100

Stritzinger M., et al. 2009, *CBET* 1751

Stritzinger M., et al. 2010, *AJ*, 140, 2036

Turatto M., Benetti S. & Cappellaro E., 2003, in the proceedings to the ESO/MPA/MPE Workshop (an ESO Astrophysics Symposium) From Twilight to Highlight: The Physics of Supernovae, eds. B. Leibundgut and W. Hillebrandt (Springer-Verlag), p. 200

Valenti S., et al. 2008, MNRAS, 383, 1485

Woosley S. E., Heger, A. 2006 ApJ, 637, 914

Yoshii Y., et al. 2003, ApJ, 592, 467

Young D. R., et al. 2010, A&A, 512, A70

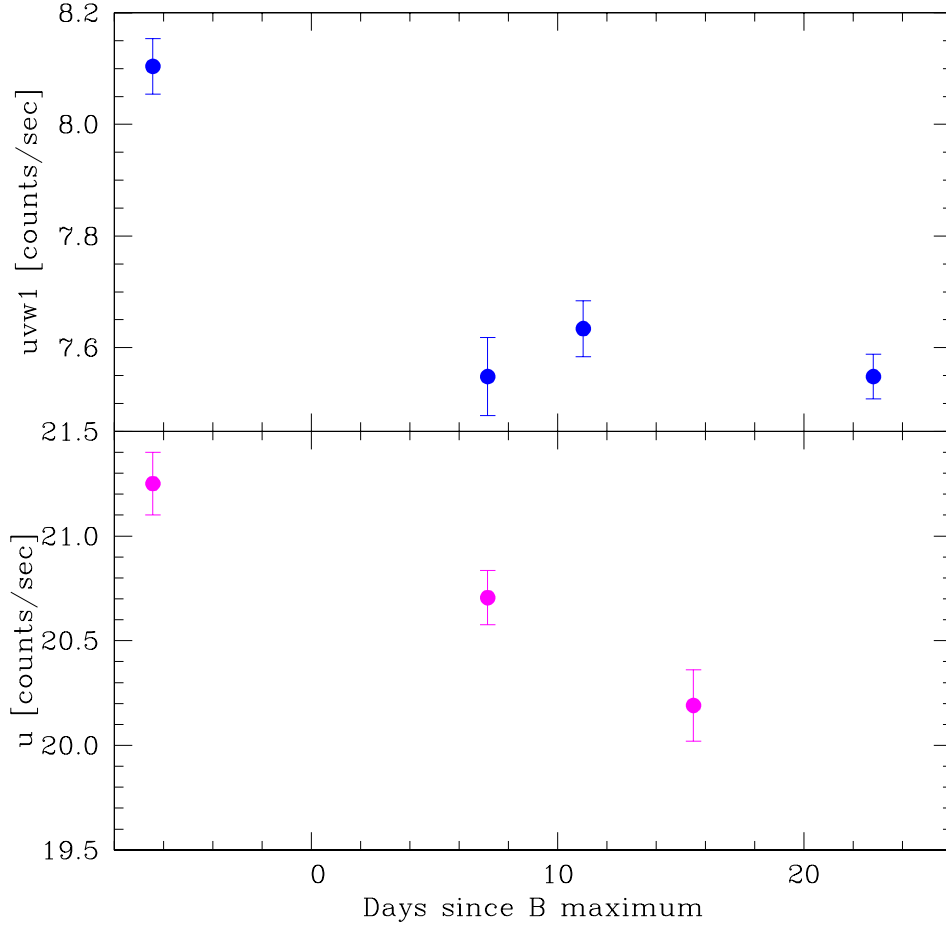


Fig. 5.— Counts rate evolution at the position of SN 2009bb in the *uvw1* (top panel) and *u* (bottom panel) bands.

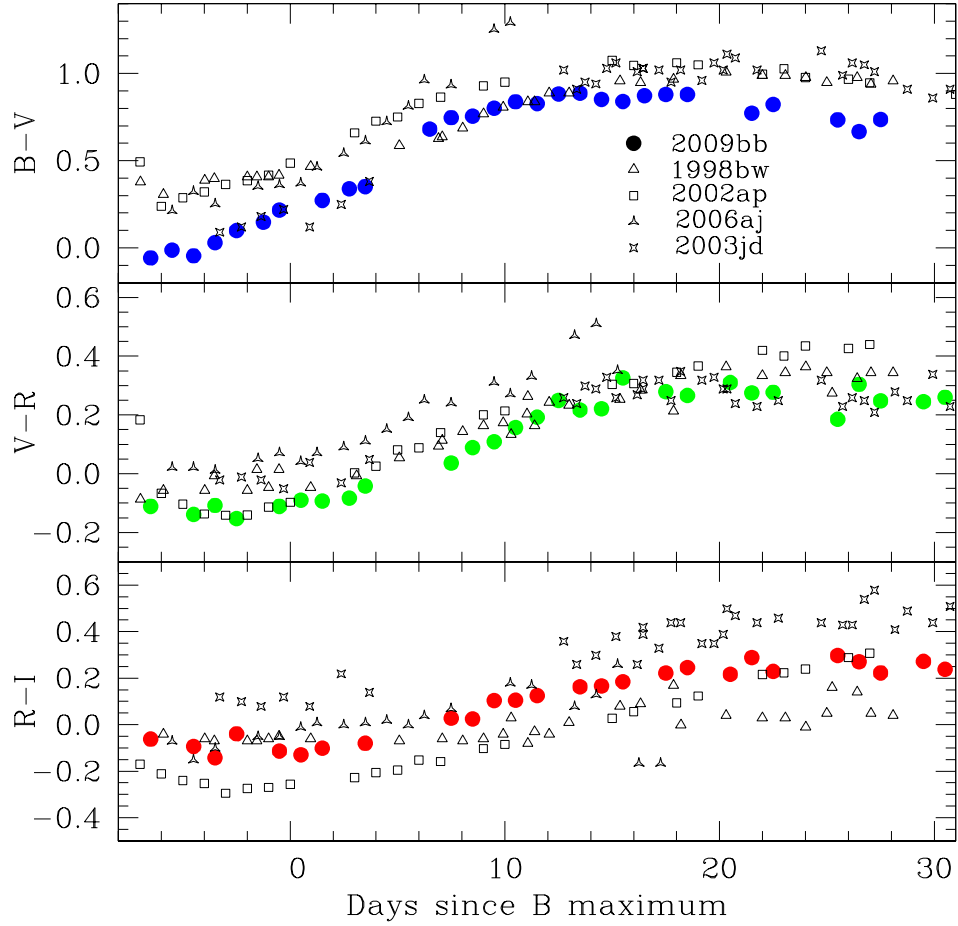


Fig. 6.— De-reddened $(B - V)_0$, $(V - R)_0$ and $(R - I)_0$ color curves of SN 2009bb. For comparison, the color curves of SN 1998bw, SN 2002ap, SN 2006aj and SN 2003jd are also shown. The bibliographic sources are the same as those given in Figure 2.

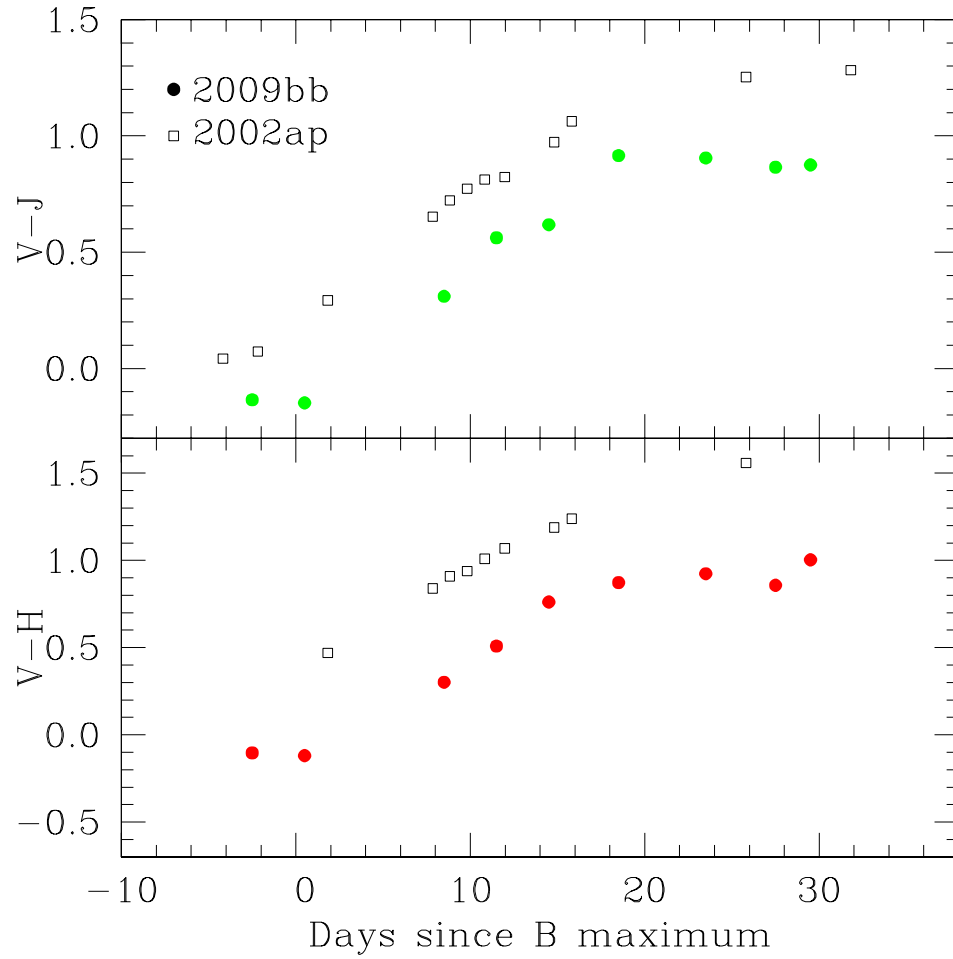


Fig. 7.— De-reddened $(V - J)_0$ and $(V - H)_0$ color curves of SN 2009bb. For comparison, the color curves of SN 2002ap are also shown. The bibliographic sources are the same as those given in Figure 4.

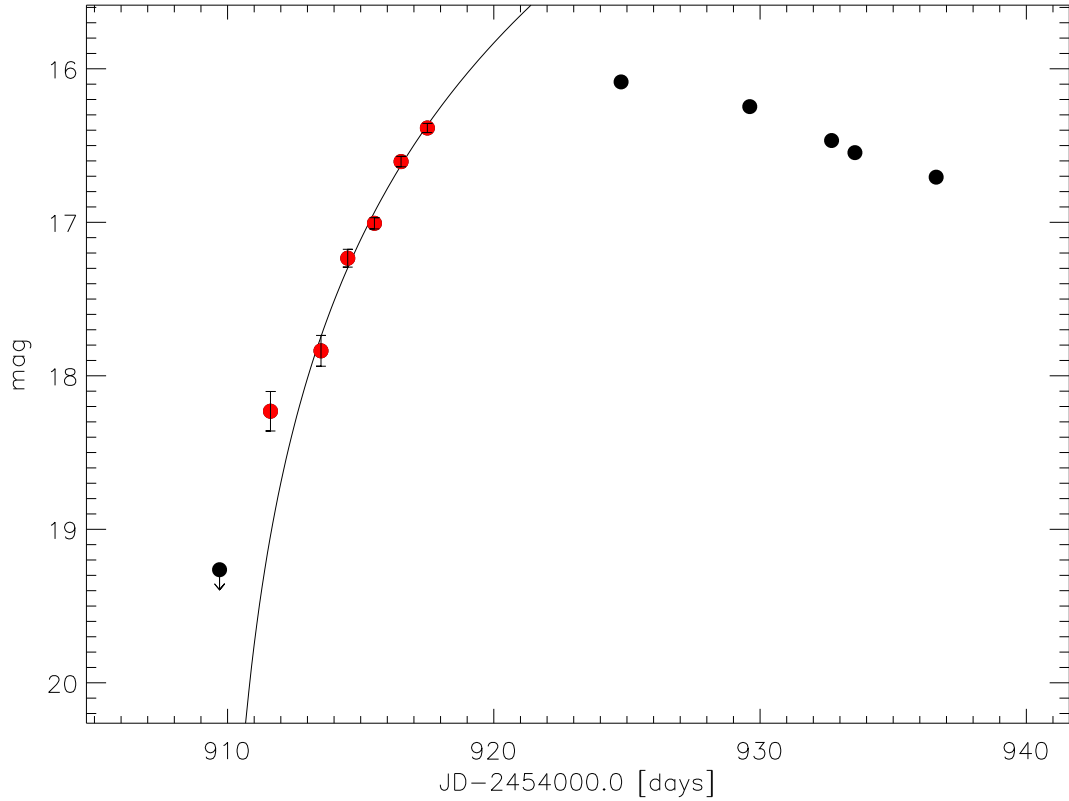


Fig. 8.— The black filled circles are the unfiltered magnitudes of SN 2009bb calibrated to the V band magnitude scale. The red filled circles are the measurements considered in the fit of the fireball model (solid line) used to estimate the SN explosion date. The first point indicates the upper-limit on the image taken immediately previous to the SN detection.

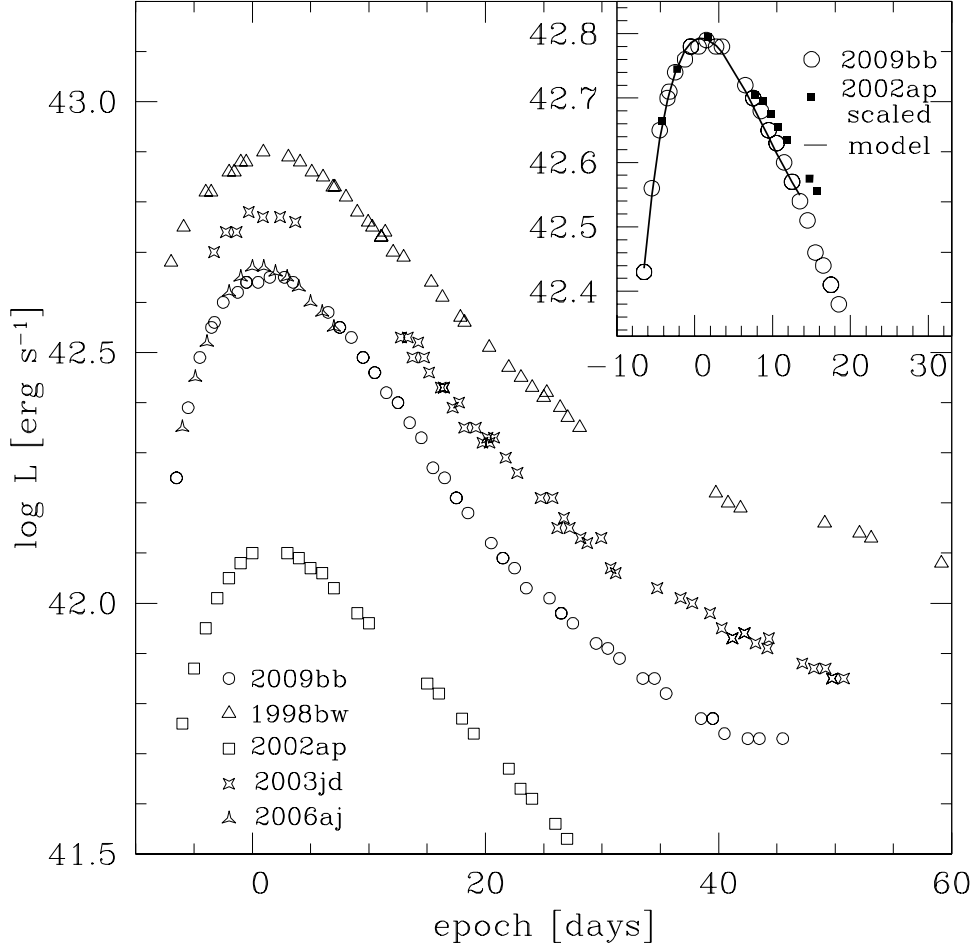


Fig. 9.— In the main plot, the pseudo-bolometric light curve of SN 2009bb obtained by combining the flux in the $BVRI$ bands is compared with those of SN 1998bw, SN 2002ap, SN 2003jd and SN 2006aj calculated in a similar way. In the inset plot, the pseudo-bolometric light curve of SN 2009bb obtained combining the flux of the $u'BVRIJH$ bands with a K band correction is shown together with the similar light curve of SN 2002ap rescaled to match SN 2009bb around maximum. The model (solid line) used to estimate the ^{56}Ni and ejecta mass for SN 2009bb is also plotted.

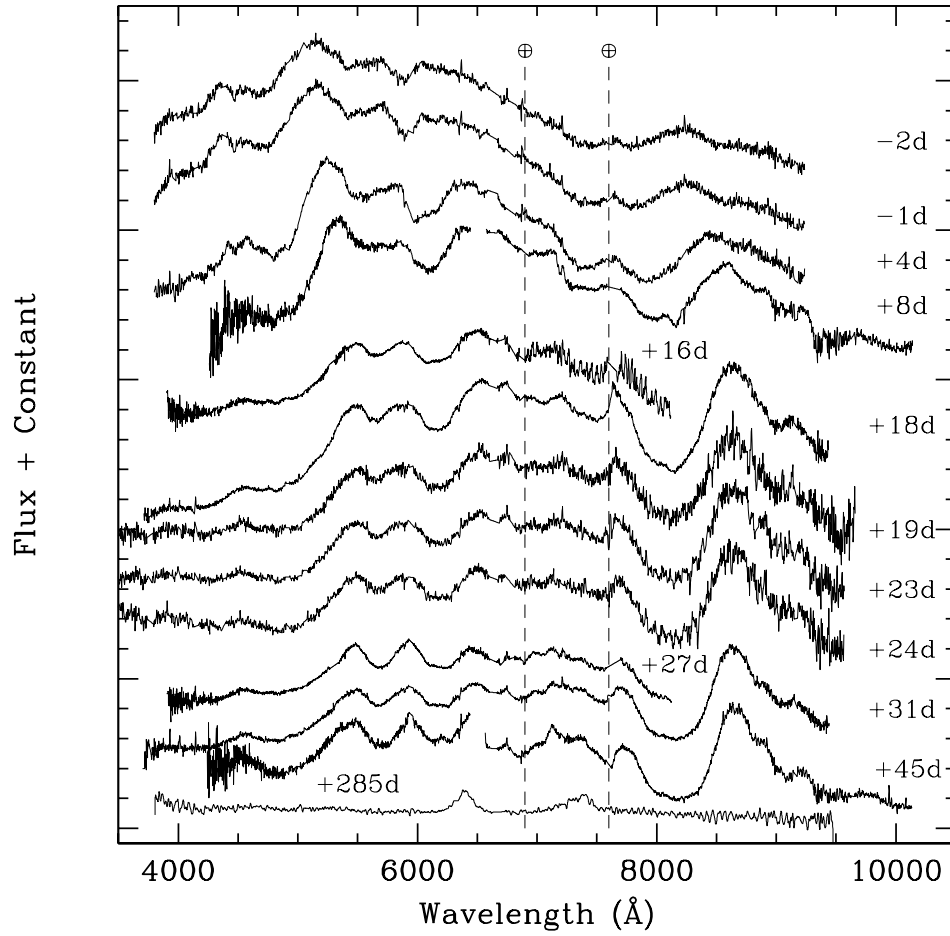


Fig. 10.— Optical spectral evolution of SN 2009bb. For presentation purposes the host galaxy emission lines have been removed and the spectra arbitrarily shifted. The \oplus symbol shows the position of the main telluric features. The spectra are labeled with the epoch in days past B maximum.

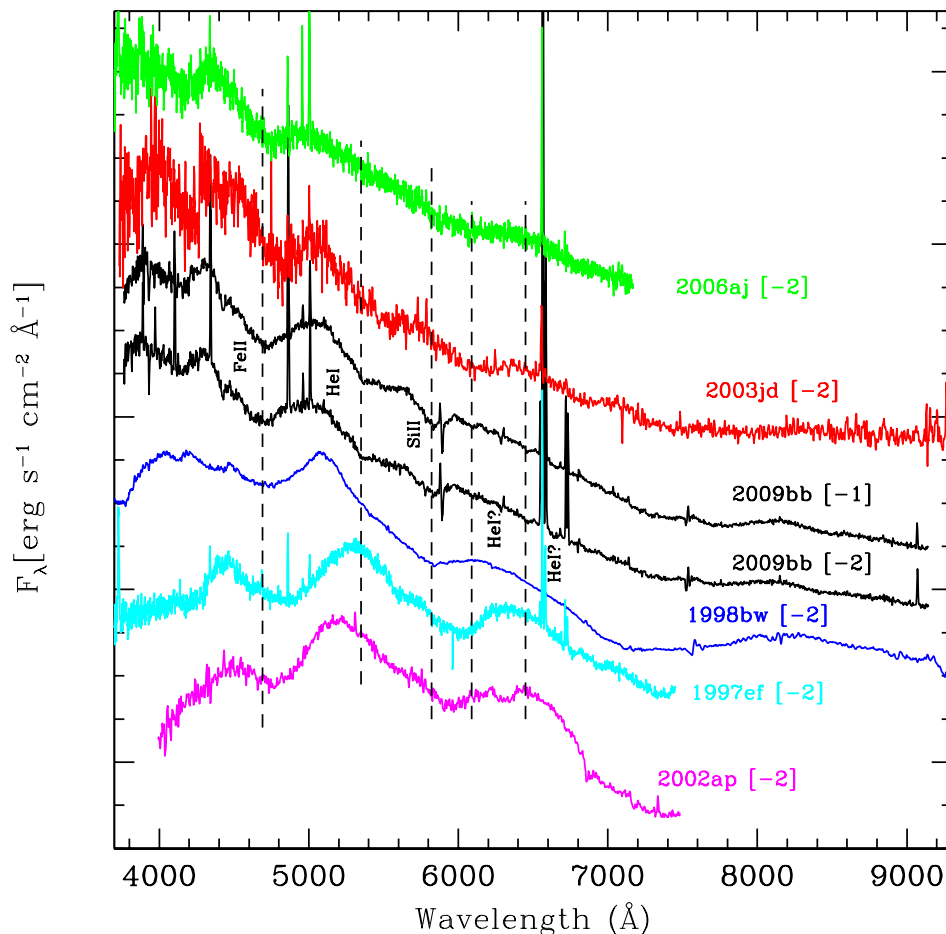


Fig. 11.— First two spectra of SN 2009bb taken before maximum light. The phase with respect to B maximum is noted in square brackets. Coeval spectra of SN 1998bw (Patat et al. 2001), SN1997ef (Matheson et al. 2001), SN 2003jd (Valenti et al. 2008), SN 2002ap (Gal-Yam, Ofek & Shemmer 2002) and SN 2006aj (Modjaz et al. 2006) are shown for comparison. The spectra have been corrected for reddening and redshift. The elements responsible for some absorption features in the SN 2009bb spectra are also labeled.

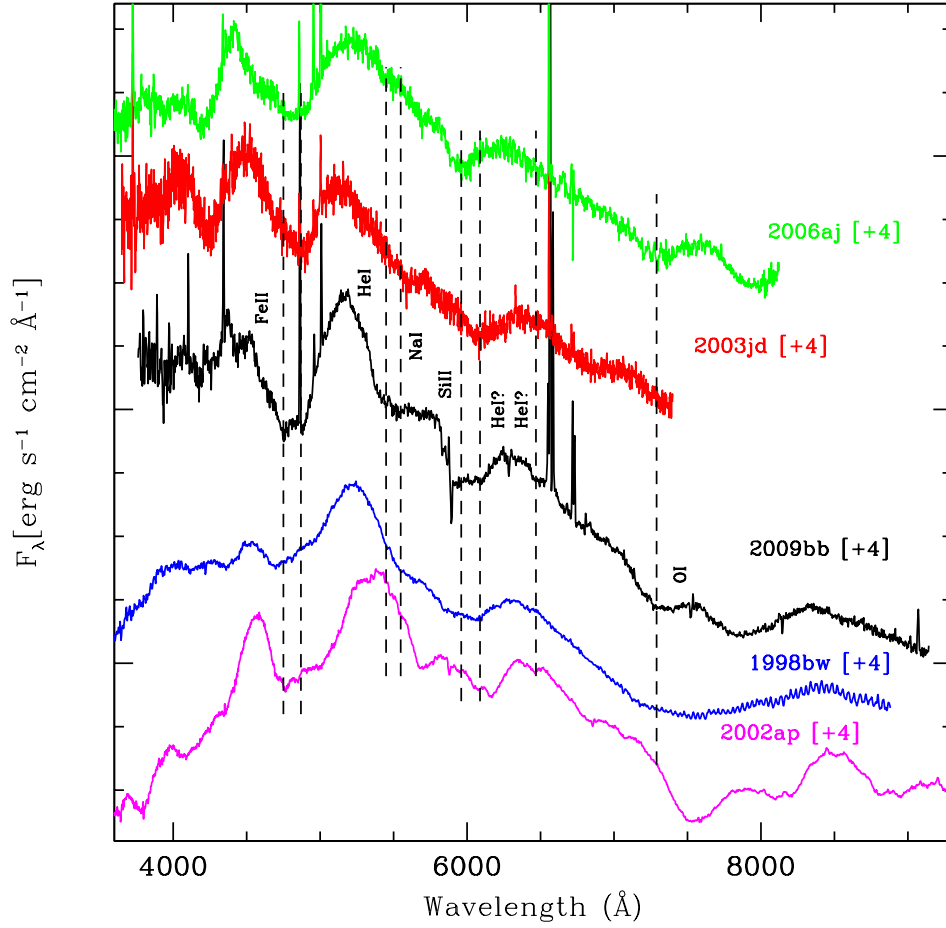


Fig. 12.— Spectrum of SN 2009bb taken 4 days after B -band maximum. The bibliographic sources for the spectra of the other SNe shown for comparison are the same as those in Figure 11.

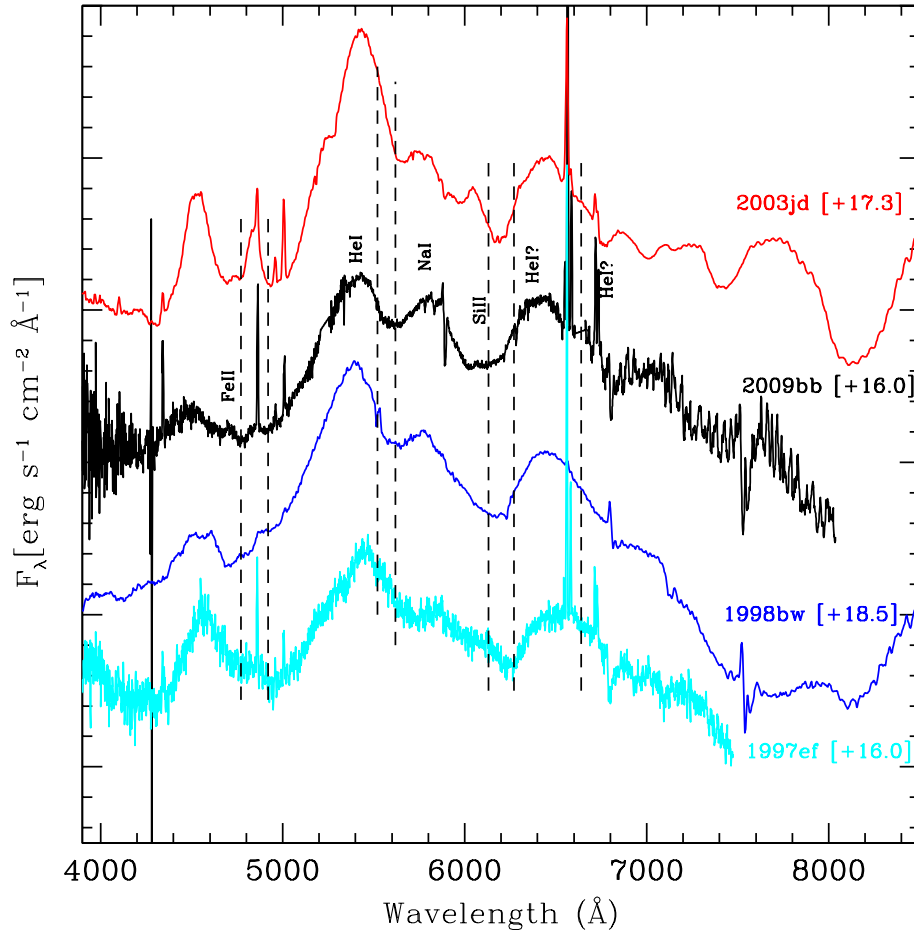


Fig. 14.— Spectrum of SN 2009bb taken 16 days after B -band maximum. The bibliographic sources for the spectra of the other SNe shown for comparison are the same as those in Figure 11.

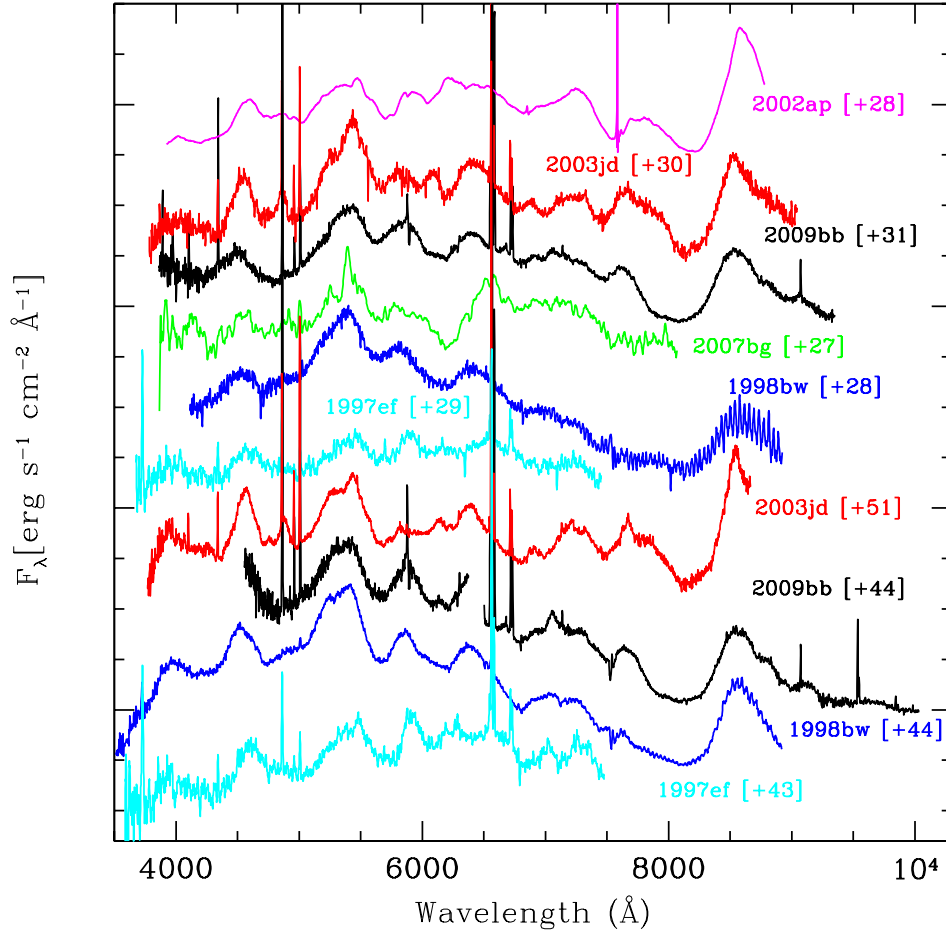


Fig. 15.— Spectra of SN 2009bb taken 30 and 44 days after B band maximum. The bibliographic sources for the spectra of the other SNe shown for comparison are the same as those in Figure 11 and Figure 13.

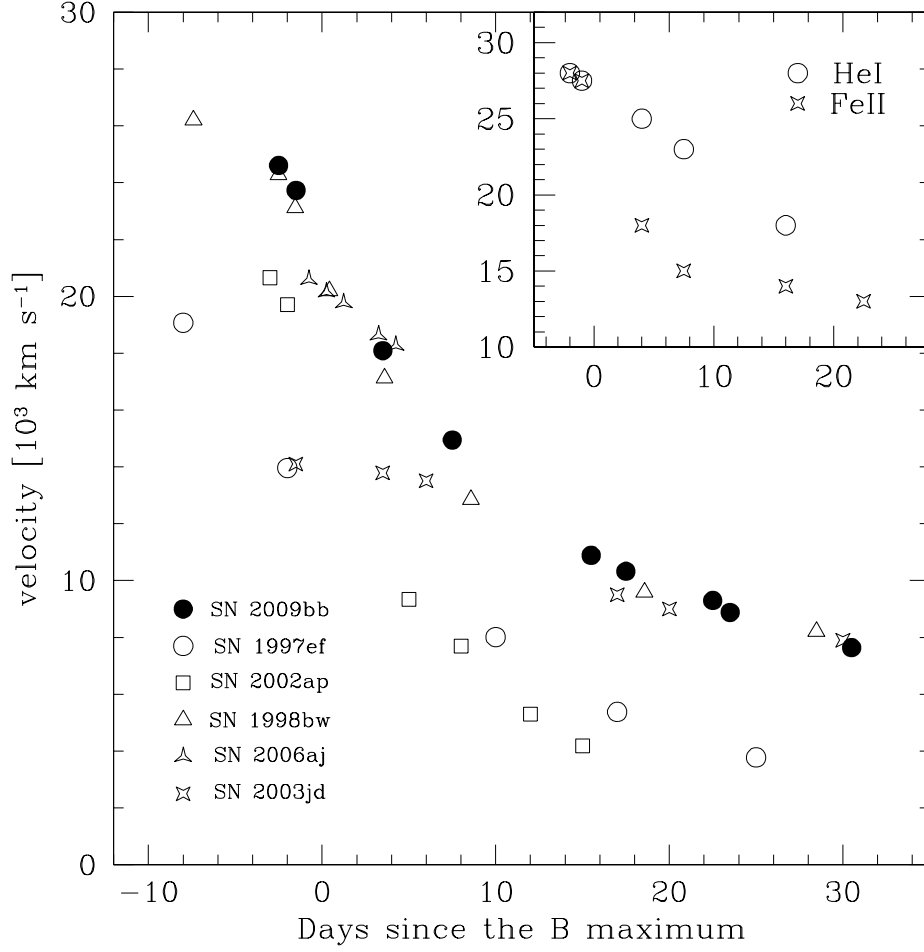


Fig. 16.— Evolution of the velocity measured from the blueshift of the minimum of Si II $\lambda 6355$ line of SN 2009bb. For comparison the Si II $\lambda 6355$ line velocities of SN 1997ef, SN 1998bw, SN 2002ap, SN 2003jd, and SN 2006aj are also reported. In the inserted plot, the velocities of the obtained fitting the Fe II $\lambda\lambda 4924, 5018, 5169$ lines with SYNOW are compared with those obtained fitting the He I lines with the same code.

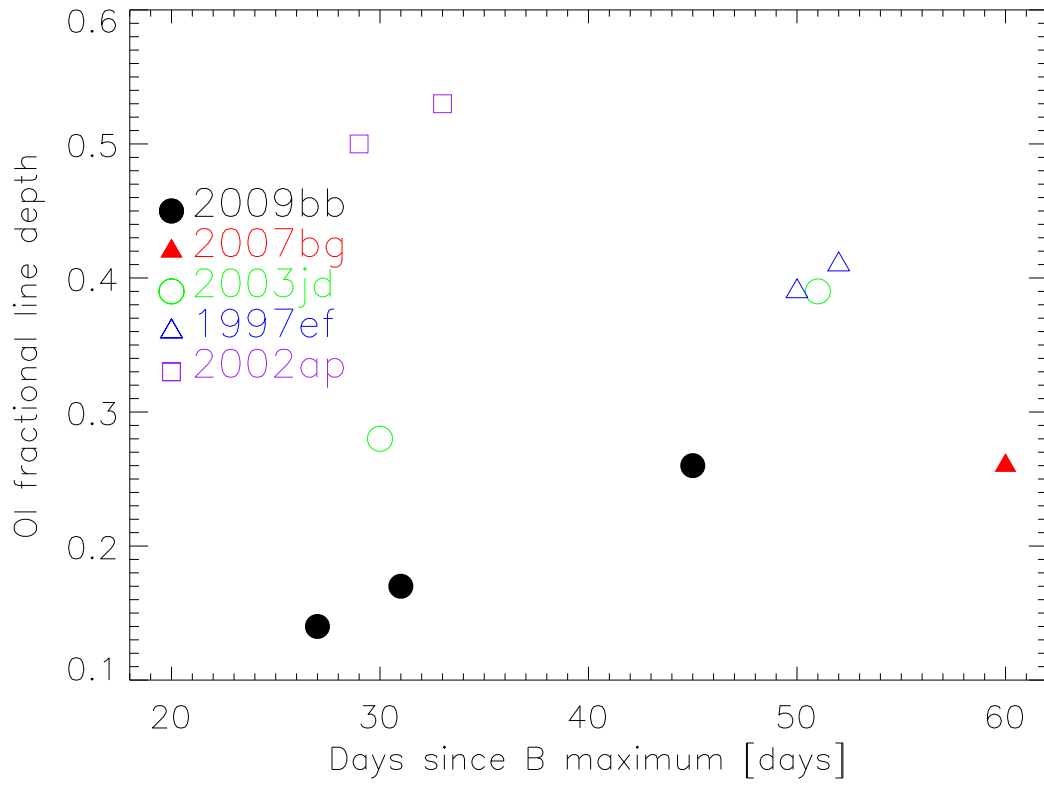


Fig. 18.— Fractional line depth of the O I $\lambda 7774$ line measured using the formula of Matheson et al. (2001).

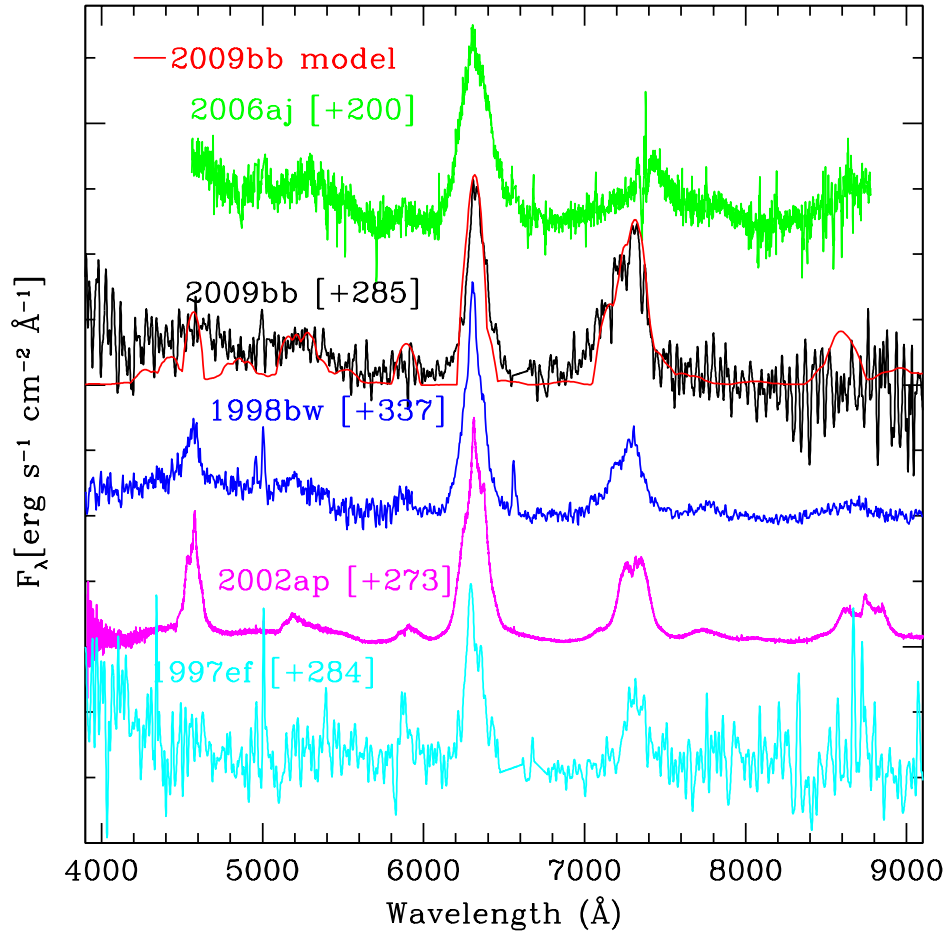


Fig. 19.— Comparison between the nebular spectra of SN 2009bb, SN 1997ef, SN 1998bw, SN 2002ap and SN 2006aj. The model spectrum of SN 2009bb discussed in Section 5.3 is also plotted.

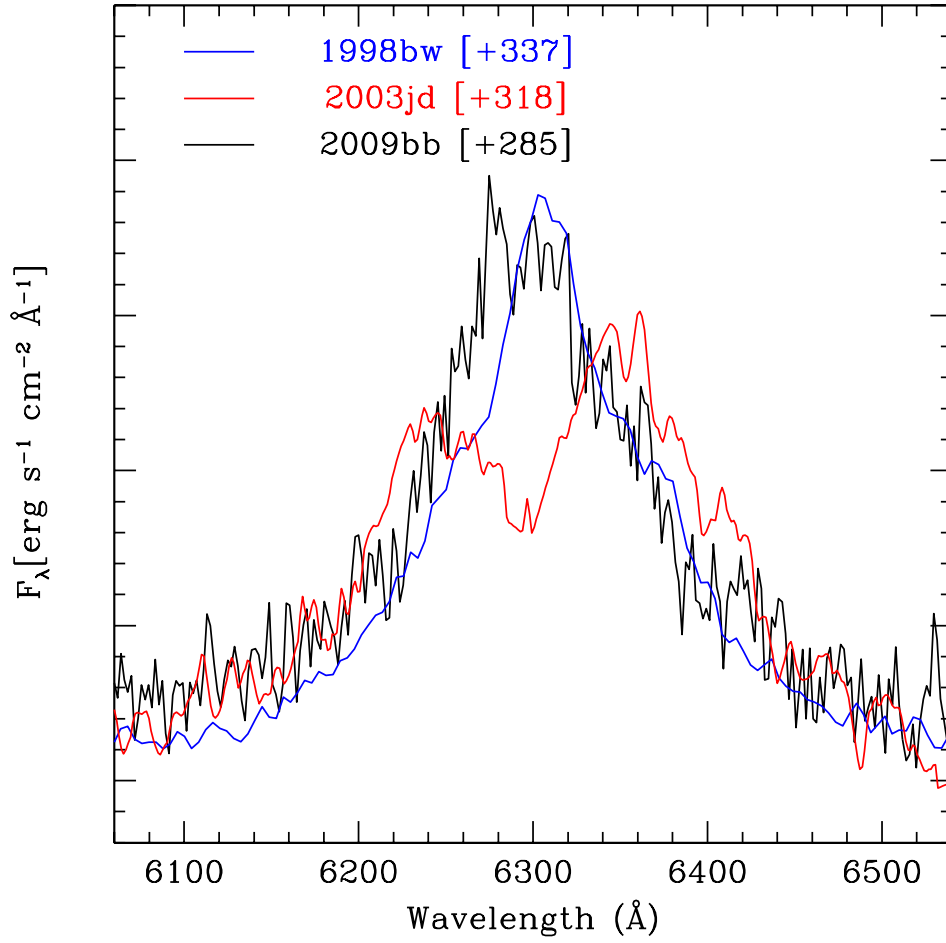


Fig. 20.— Comparison between the [O I] $\lambda\lambda 6300, 6354$ nebular emission lines of SN 2009bb, SN 1998bw and SN 2003jd.

Table 1. *BVRI* photometry of SN 2009bb

date	J.D.	<i>B</i>	<i>V</i>	<i>R</i>	<i>I</i>	Telescope
24/3/2009	2454914.5	18.10 ± 0.06	–	–	–	PROMPT3
24/3/2009	2454914.5	–	17.21 ± 0.06	17.09 ± 0.03	16.75 ± 0.08	PROMPT5
24/3/2009	2454914.6	18.00 ± 0.1	–	–	–	Swope
25/3/2009	2454915.6	17.49 ± 5.27	16.82 ± 0.1	–	–	Swope
26/3/2009	2454916.5	17.33 ± 0.04	–	–	–	PROMPT3
26/3/2009	2454916.5	–	16.65 ± 0.04	16.36 ± 0.03	15.95 ± 0.05	PROMPT5
27/3/2009	2454917.5	17.21 ± 0.03	–	–	–	PROMPT3
27/3/2009	2454917.5	–	16.48 ± 0.04	16.15 ± 0.03	15.80 ± 0.05	PROMPT5
27/3/2009	2454917.7	17.17 ± 0.04	16.40 ± 0.1	–	–	Swope
28/3/2009	2454918.5	17.13 ± 0.04	–	–	–	PROMPT3
28/3/2009	2454918.5	–	16.34 ± 0.03	16.05 ± 0.03	–	PROMPT5
28/3/2009	2454918.6	–	–	–	15.71 ± 0.04	PROMPT5
29/3/2009	2454919.7	17.08 ± 0.04	–	–	–	PROMPT3
29/3/2009	2454919.7	–	16.21 ± 0.03	–	15.59 ± 0.06	PROMPT5
30/3/2009	2454920.5	17.07 ± 0.04	–	–	–	PROMPT3
30/3/2009	2454920.5	–	16.21 ± 0.04	15.90 ± 0.03	15.50 ± 0.05	PROMPT5
30/3/2009	2454920.6	17.07 ± 0.03	16.16 ± 0.1	–	–	Swope
31/3/2009	2454921.5	–	16.10 ± 0.03	15.85 ± 0.03	15.49 ± 0.05	PROMPT5
1/4/2009	2454922.5	17.07 ± 0.03	–	–	–	PROMPT3
1/4/2009	2454922.5	–	16.08 ± 0.03	15.81 ± 0.03	15.42 ± 0.06	PROMPT5
2/4/2009	2454923.6	–	–	–	15.35 ± 0.04	PROMPT5
2/4/2009	2454923.7	17.16 ± 0.04	–	–	–	PROMPT3
2/4/2009	2454923.7	–	16.07 ± 0.03	15.79 ± 0.03	–	PROMPT5
3/4/2009	2454924.5	17.25 ± 0.04	–	–	–	PROMPT3
3/4/2009	2454924.6	–	16.08 ± 0.03	15.78 ± 0.03	15.35 ± 0.06	PROMPT5
6/4/2009	2454927.6	17.57 ± 0.27	16.21 ± 0.1	–	–	Swope
7/4/2009	2454928.5	17.78 ± 0.03	–	–	–	PROMPT3
7/4/2009	2454928.5	–	16.31 ± 0.03	15.85 ± 0.04	15.37 ± 0.04	PROMPT5
7/4/2009	2454928.6	17.75 ± 0.07	16.31 ± 0.1	–	–	Swope
8/4/2009	2454929.5	17.84 ± 0.04	–	–	–	PROMPT3
8/4/2009	2454929.5	–	16.41 ± 0.04	15.90 ± 0.03	15.37 ± 0.05	PROMPT5
9/4/2009	2454930.5	18.00 ± 0.07	16.50 ± 0.1	–	–	Swope

Table 1—Continued

date	J.D.	<i>B</i>	<i>V</i>	<i>R</i>	<i>I</i>	Telescope
9/4/2009	2454930.5	18.02 ± 0.05	–	–	–	PROMPT3
9/4/2009	2454930.5	–	16.52 ± 0.04	16.00 ± 0.03	15.40 ± 0.05	PROMPT5
10/4/2009	2454931.5	–	16.59 ± 0.04	16.01 ± 0.03	15.44 ± 0.04	PROMPT5
10/4/2009	2454931.6	18.13 ± 0.05	16.56 ± 0.1	–	–	Swope
11/4/2009	2454932.5	–	16.71 ± 0.04	16.10 ± 0.03	15.48 ± 0.05	PROMPT5
12/4/2009	2454933.5	–	16.76 ± 0.05	16.14 ± 0.03	–	PROMPT5
12/4/2009	2454933.6	18.40 ± 0.10	16.75 ± 0.1	–	–	Swope
13/4/2009	2454934.5	18.48 ± 0.05	–	–	–	PROMPT3
13/4/2009	2454934.5	–	16.90 ± 0.04	16.22 ± 0.05	15.59 ± 0.04	PROMPT5
14/4/2009	2454935.5	18.59 ± 0.06	–	–	–	PROMPT3
14/4/2009	2454935.5	–	16.95 ± 0.05	16.33 ± 0.03	15.67 ± 0.05	PROMPT5
15/4/2009	2454936.5	18.67 ± 0.05	–	–	–	PROMPT3
15/4/2009	2454936.5	–	17.11 ± 0.05	16.43 ± 0.03	15.74 ± 0.04	PROMPT5
16/4/2009	2454937.6	18.81 ± 0.09	17.15 ± 0.1	–	–	Swope
17/4/2009	2454938.5	–	17.25 ± 0.06	16.60 ± 0.03	15.89 ± 0.05	PROMPT5
17/4/2009	2454938.6	18.92 ± 0.14	17.22 ± 0.1	–	–	Swope
18/4/2009	2454939.5	–	17.35 ± 0.06	16.68 ± 0.03	15.96 ± 0.05	PROMPT5
20/4/2009	2454941.6	–	17.54 ± 0.06	16.82 ± 0.03	16.12 ± 0.05	PROMPT5
21/4/2009	2454942.5	–	17.54 ± 0.07	16.92 ± 0.03	16.16 ± 0.05	PROMPT5
21/4/2009	2454942.6	19.16 ± 0.12	17.51 ± 0.1	–	–	Swope
22/4/2009	2454943.5	–	17.62 ± 0.07	16.96 ± 0.04	16.23 ± 0.05	PROMPT5
23/4/2009	2454944.6	–	17.67 ± 0.06	–	16.38 ± 0.05	PROMPT5
23/4/2009	2454944.7	19.38 ± 0.10	–	–	–	PROMPT3
25/4/2009	2454946.5	19.38 ± 0.09	–	–	–	PROMPT3
25/4/2009	2454946.5	–	17.74 ± 0.07	–	–	PROMPT5
25/4/2009	2454946.6	–	–	17.18 ± 0.03	16.45 ± 0.06	PROMPT5
26/4/2009	2454947.5	–	17.80 ± 0.1	–	–	Swope
26/4/2009	2454947.5	–	–	–	16.47 ± 0.05	PROMPT5
26/4/2009	2454947.6	19.43 ± 0.19	–	–	–	Swope
26/4/2009	2454947.6	–	17.85 ± 0.08	17.20 ± 0.03	–	PROMPT5
27/4/2009	2454948.6	–	17.88 ± 0.07	17.24 ± 0.03	16.54 ± 0.06	PROMPT5
29/4/2009	2454950.5	–	–	17.33 ± 0.03	–	PROMPT5

Table 1—Continued

date	J.D.	<i>B</i>	<i>V</i>	<i>R</i>	<i>I</i>	Telescope
29/4/2009	2454950.6	–	17.95 ± 0.11	–	16.60 ± 0.07	PROMPT5
30/4/2009	2454951.5	–	17.99 ± 0.10	17.35 ± 0.04	16.61 ± 0.08	PROMPT5
1/5/2009	2454952.5	–	18.07 ± 0.11	17.39 ± 0.03	16.64 ± 0.07	PROMPT5
2/5/2009	2454953.5	19.48 ± 0.04	–	–	–	PROMPT3
3/5/2009	2454954.5	–	18.15 ± 0.10	17.50 ± 0.04	16.73 ± 0.07	PROMPT5
4/5/2009	2454955.5	–	18.16 ± 0.11	17.50 ± 0.03	16.81 ± 0.08	PROMPT5
5/5/2009	2454956.5	19.93 ± 0.49	–	–	–	PROMPT3
5/5/2009	2454956.5	–	18.30 ± 0.11	17.63 ± 0.03	16.87 ± 0.06	PROMPT5
8/5/2009	2454959.5	19.70 ± 0.20	–	–	–	PROMPT3
8/5/2009	2454959.5	–	18.21 ± 0.09	17.70 ± 0.03	16.95 ± 0.08	PROMPT5
9/5/2009	2454960.5	19.81 ± 0.13	18.23 ± 0.1	–	–	Swope
9/5/2009	2454960.5	19.88 ± 0.14	–	–	–	PROMPT3
9/5/2009	2454960.5	–	18.21 ± 0.11	17.72 ± 0.03	–	PROMPT5
9/5/2009	2454960.6	–	–	–	16.86 ± 0.08	PROMPT5
10/5/2009	2454961.6	20.08 ± 0.16	–	–	–	PROMPT3
10/5/2009	2454961.6	–	18.36 ± 0.12	17.79 ± 0.03	17.06 ± 0.10	PROMPT5
11/5/2009	2454962.5	19.86 ± 0.27	–	–	–	PROMPT3
11/5/2009	2454962.5	–	18.31 ± 0.14	17.71 ± 0.04	16.94 ± 0.07	PROMPT5
12/5/2009	2454963.5	19.64 ± 0.27	–	–	–	PROMPT3
12/5/2009	2454963.5	–	18.41 ± 0.14	17.95 ± 0.03	17.08 ± 0.05	PROMPT5
13/5/2009	2454964.5	19.91 ± 0.29	–	–	–	PROMPT3
13/5/2009	2454964.5	–	18.75 ± 0.17	17.90 ± 0.03	–	PROMPT5
13/5/2009	2454964.6	19.96 ± 0.1	18.34 ± 0.1	–	–	Swope
15/5/2009	2454966.5	20.03 ± 0.1	18.48 ± 0.1	–	–	Swope
16/5/2009	2454967.5	–	18.29 ± 0.09	17.99 ± 0.03	16.93 ± 0.09	PROMPT5
17/5/2009	2454968.5	–	18.46 ± 0.13	17.98 ± 0.04	17.21 ± 0.11	PROMPT5
19/5/2009	2454970.5	–	18.49 ± 0.15	17.98 ± 0.06	17.39 ± 0.12	PROMPT5
21/5/2009	2454972.5	–	18.99 ± 0.18	18.14 ± 0.03	17.33 ± 0.11	PROMPT5
22/5/2009	2454973.5	–	18.72 ± 0.18	18.11 ± 0.03	17.35 ± 0.11	PROMPT5
2/6/2009	2454984.5	–	18.95 ± 0.19	18.57 ± 0.05	–	PROMPT5
2/6/2009	2454984.6	–	–	–	17.47 ± 0.17	PROMPT5
11/6/2009	2454993.5	–	19.14 ± 0.17	18.58 ± 0.03	18.11 ± 0.20	PROMPT5

Table 1—Continued

date	J.D.	<i>B</i>	<i>V</i>	<i>R</i>	<i>I</i>	Telescope
12/6/2009	2454994.5	–	–	18.90 ± 0.03	–	PROMPT5
12/6/2009	2454994.6	–	–	–	18.00 ± 0.23	PROMPT5
13/6/2009	2454995.5	–	19.59 ± 0.29	18.84 ± 0.04	18.00 ± 0.17	PROMPT5
25/7/2009	2455037.5	–	19.78 ± 0.78	–	–	PROMPT5

Table 2. $u'g'r'i'z'$ photometry of SN 2009bb

date	J.D.	u'	g'	r'	i'	z'	Telescope
24/3/2009	2454914.5	–	–	17.33 ± 0.03	17.24 ± 0.05	17.12 ± 0.08	PROMPT5
24/3/2009	2454914.5	–	17.58 ± 0.06	–	–	–	PROMPT3
24/3/2009	2454914.6	18.84 ± 0.1	17.59 ± 0.1	17.23 ± 0.1	17.10 ± 0.1	–	Swope
25/3/2009	2454915.6	18.43 ± 0.1	17.21 ± 0.03	16.82 ± 0.03	16.71 ± 0.05	–	Swope
26/3/2009	2454916.5	–	–	16.55 ± 0.03	16.44 ± 0.03	16.38 ± 0.07	PROMPT5
26/3/2009	2454916.5	–	16.99 ± 0.05	–	–	–	PROMPT3
27/3/2009	2454917.5	–	–	16.35 ± 0.03	16.25 ± 0.03	16.07 ± 0.06	PROMPT5
27/3/2009	2454917.5	–	16.84 ± 0.04	–	–	–	PROMPT3
27/3/2009	2454917.7	18.13 ± 0.1	16.82 ± 0.03	16.32 ± 0.03	16.27 ± 0.04	–	Swope
28/3/2009	2454918.5	–	–	16.20 ± 0.03	16.18 ± 0.03	15.95 ± 0.07	PROMPT5
28/3/2009	2454918.5	–	16.72 ± 0.04	–	–	–	PROMPT3
29/3/2009	2454919.7	–	16.66 ± 0.04	–	–	–	PROMPT3
30/3/2009	2454920.5	–	–	16.06 ± 0.03	16.03 ± 0.03	15.80 ± 0.06	PROMPT5
30/3/2009	2454920.5	–	16.62 ± 0.04	–	–	–	PROMPT3
30/3/2009	2454920.6	18.11 ± 0.1	16.63 ± 0.03	16.07 ± 0.03	16.00 ± 0.04	–	Swope
31/3/2009	2454921.5	–	–	16.03 ± 0.03	16.00 ± 0.03	15.78 ± 0.06	PROMPT5
1/4/2009	2454922.5	–	–	16.02 ± 0.03	15.95 ± 0.03	15.69 ± 0.06	PROMPT5
1/4/2009	2454922.5	–	16.65 ± 0.04	–	–	–	PROMPT3
2/4/2009	2454923.6	–	–	15.96 ± 0.03	15.91 ± 0.03	15.63 ± 0.07	PROMPT5
2/4/2009	2454923.7	–	16.69 ± 0.04	–	–	–	PROMPT3
3/4/2009	2454924.5	–	–	15.98 ± 0.03	15.91 ± 0.03	15.60 ± 0.06	PROMPT5
3/4/2009	2454924.5	–	16.70 ± 0.04	–	–	–	PROMPT3
6/4/2009	2454927.6	18.98 ± 0.1	16.97 ± 0.03	16.02 ± 0.04	15.90 ± 0.03	–	Swope
7/4/2009	2454928.5	19.27 ± 0.1	17.09 ± 0.03	16.05 ± 0.03	15.93 ± 0.03	–	Swope
7/4/2009	2454928.5	–	–	16.07 ± 0.03	15.93 ± 0.03	15.60 ± 0.06	PROMPT5
7/4/2009	2454928.5	–	17.05 ± 0.04	–	–	–	PROMPT3
8/4/2009	2454929.5	–	–	16.14 ± 0.03	15.96 ± 0.03	15.70 ± 0.06	PROMPT5
8/4/2009	2454929.5	–	17.14 ± 0.05	–	–	–	PROMPT3
9/4/2009	2454930.5	19.62 ± 0.1	17.30 ± 0.03	16.16 ± 0.04	16.00 ± 0.04	–	Swope
9/4/2009	2454930.5	–	–	16.15 ± 0.03	16.00 ± 0.04	15.64 ± 0.07	PROMPT5
9/4/2009	2454930.5	–	17.30 ± 0.05	–	–	–	PROMPT3
10/4/2009	2454931.5	19.71 ± 0.1	17.42 ± 0.03	16.22 ± 0.03	16.05 ± 0.03	–	Swope

Table 2—Continued

date	J.D.	u'	g'	r'	i'	z'	Telescope
10/4/2009	2454931.5	–	–	16.22 ± 0.03	16.05 ± 0.03	15.69 ± 0.06	PROMPT5
10/4/2009	2454931.5	–	17.38 ± 0.05	–	–	–	PROMPT3
11/4/2009	2454932.5	–	–	16.34 ± 0.03	16.09 ± 0.03	15.73 ± 0.06	PROMPT5
11/4/2009	2454932.5	–	17.52 ± 0.05	–	–	–	PROMPT3
12/4/2009	2454933.5	20.03 ± 0.1	17.67 ± 0.03	16.37 ± 0.03	16.15 ± 0.04	–	Swope
12/4/2009	2454933.5	–	–	16.40 ± 0.03	–	15.77 ± 0.06	PROMPT5
12/4/2009	2454933.5	–	17.62 ± 0.05	–	–	–	PROMPT3
13/4/2009	2454934.5	–	–	16.48 ± 0.03	16.25 ± 0.03	15.85 ± 0.06	PROMPT5
13/4/2009	2454934.5	–	17.72 ± 0.07	–	–	–	PROMPT3
14/4/2009	2454935.5	–	–	16.55 ± 0.03	16.30 ± 0.04	15.90 ± 0.06	PROMPT5
14/4/2009	2454935.5	–	17.92 ± 0.07	–	–	–	PROMPT3
15/4/2009	2454936.5	–	–	16.69 ± 0.03	16.41 ± 0.04	15.96 ± 0.06	PROMPT5
15/4/2009	2454936.5	–	18.07 ± 0.08	–	–	–	PROMPT3
16/4/2009	2454937.6	20.51 ± 0.1	18.15 ± 0.03	16.75 ± 0.03	16.49 ± 0.04	–	Swope
17/4/2009	2454938.5	–	–	16.84 ± 0.03	16.61 ± 0.04	16.10 ± 0.06	PROMPT5
17/4/2009	2454938.6	20.48 ± 0.1	18.25 ± 0.03	16.86 ± 0.03	16.58 ± 0.03	–	Swope
18/4/2009	2454939.5	–	–	16.96 ± 0.03	16.63 ± 0.04	16.16 ± 0.06	PROMPT5
18/4/2009	2454939.5	–	18.30 ± 0.10	–	–	–	PROMPT3
20/4/2009	2454941.6	–	–	17.10 ± 0.03	16.81 ± 0.04	16.31 ± 0.07	PROMPT5
20/4/2009	2454941.6	–	18.55 ± 0.13	–	–	–	PROMPT3
21/4/2009	2454942.5	–	–	17.23 ± 0.03	16.83 ± 0.04	16.36 ± 0.07	PROMPT5
21/4/2009	2454942.5	–	18.62 ± 0.13	–	–	–	PROMPT3
21/4/2009	2454942.6	20.65 ± 0.1	18.55 ± 0.03	17.16 ± 0.03	16.89 ± 0.06	–	Swope
22/4/2009	2454943.5	–	–	17.27 ± 0.03	16.94 ± 0.04	16.41 ± 0.07	PROMPT5
22/4/2009	2454943.5	–	18.67 ± 0.13	–	–	–	PROMPT3
23/4/2009	2454944.6	–	–	17.38 ± 0.04	–	16.52 ± 0.07	PROMPT5
23/4/2009	2454944.6	–	18.80 ± 0.15	–	–	–	PROMPT3
25/4/2009	2454946.5	–	18.83 ± 0.16	–	–	–	PROMPT3
25/4/2009	2454946.6	–	–	17.47 ± 0.03	17.08 ± 0.04	16.53 ± 0.07	PROMPT5
26/4/2009	2454947.5	21.05 ± 0.1	18.98 ± 0.06	17.54 ± 0.03	17.24 ± 0.05	–	Swope
26/4/2009	2454947.5	–	–	17.48 ± 0.03	17.21 ± 0.05	16.58 ± 0.07	PROMPT5
26/4/2009	2454947.5	–	18.98 ± 0.14	–	–	–	PROMPT3

Table 2—Continued

date	J.D.	u'	g'	r'	i'	z'	Telescope
27/4/2009	2454948.5	–	18.98 ± 0.18	–	–	–	PROMPT3
27/4/2009	2454948.6	–	–	17.56 ± 0.04	17.24 ± 0.05	16.68 ± 0.07	PROMPT5
28/4/2009	2454949.5	–	19.06 ± 0.19	–	–	–	PROMPT3
29/4/2009	2454950.5	–	–	–	–	16.71 ± 0.08	PROMPT5
29/4/2009	2454950.6	–	–	17.69 ± 0.04	17.38 ± 0.05	–	PROMPT5
29/4/2009	2454950.6	–	19.12 ± 0.20	–	–	–	PROMPT3
30/4/2009	2454951.5	–	–	17.75 ± 0.04	17.43 ± 0.05	16.79 ± 0.08	PROMPT5
30/4/2009	2454951.5	–	19.29 ± 0.20	–	–	–	PROMPT3
1/5/2009	2454952.5	–	–	17.83 ± 0.04	17.50 ± 0.05	16.79 ± 0.08	PROMPT5
1/5/2009	2454952.5	–	19.32 ± 0.23	–	–	–	PROMPT3
2/5/2009	2454953.5	–	19.26 ± 0.18	–	–	–	PROMPT3
3/5/2009	2454954.5	–	–	17.88 ± 0.03	17.61 ± 0.06	16.90 ± 0.08	PROMPT5
3/5/2009	2454954.5	–	19.37 ± 0.17	–	–	–	PROMPT3
4/5/2009	2454955.5	–	–	17.93 ± 0.04	17.57 ± 0.05	16.85 ± 0.09	PROMPT5
5/5/2009	2454956.5	–	–	17.97 ± 0.06	–	16.96 ± 1.84	PROMPT5
8/5/2009	2454959.5	–	–	18.17 ± 0.05	17.70 ± 0.06	17.08 ± 0.10	PROMPT5
8/5/2009	2454959.5	–	19.46 ± 0.20	–	–	–	PROMPT3
9/5/2009	2454960.5	21.62 ± 0.1	19.49 ± 0.03	18.20 ± 0.07	17.80 ± 0.07	–	Swope
9/5/2009	2454960.5	–	–	18.18 ± 0.06	17.69 ± 0.05	–	PROMPT5
9/5/2009	2454960.5	–	19.43 ± 0.46	–	–	–	PROMPT3
9/5/2009	2454960.6	–	–	–	–	17.04 ± 0.08	PROMPT5
10/5/2009	2454961.5	–	–	18.12 ± 0.04	–	–	PROMPT5
10/5/2009	2454961.6	–	–	–	17.84 ± 0.07	17.11 ± 0.07	PROMPT5
10/5/2009	2454961.6	–	19.53 ± 0.28	–	–	–	PROMPT3
11/5/2009	2454962.5	–	–	–	17.86 ± 0.06	17.07 ± 0.09	PROMPT5
12/5/2009	2454963.5	–	–	18.19 ± 0.04	17.89 ± 0.05	17.17 ± 0.11	PROMPT5
13/5/2009	2454964.5	–	19.51 ± 0.33	–	–	–	PROMPT3
13/5/2009	2454964.6	21.61 ± 0.1	19.59 ± 0.04	18.30 ± 0.05	17.96 ± 0.10	–	Swope
15/5/2009	2454966.5	–	19.65 ± 0.15	18.43 ± 0.19	18.00 ± 0.07	–	Swope
17/5/2009	2454968.5	–	19.88 ± 0.70	–	–	–	PROMPT3
21/5/2009	2454972.5	–	–	18.60 ± 0.06	18.22 ± 0.08	17.48 ± 0.10	PROMPT5
22/5/2009	2454973.6	–	–	18.51 ± 0.05	18.29 ± 0.09	17.53 ± 0.10	PROMPT5

Table 2—Continued

date	J.D.	u'	g'	r'	i'	z'	Telescope
22/5/2009	2454973.6	–	19.95 ± 0.48	–	–	–	PROMPT3
23/5/2009	2454974.5	–	–	18.69 ± 0.07	18.25 ± 0.07	17.63 ± 0.13	PROMPT5

Table 3: YJH photometry of SN 2009bb

date	J.D.	Y	J	H	Instr.
31/3/2009	2454921.7	15.21 ± 0.04	15.08 ± 0.04	14.89 ± 0.04	RetroCam
8/4/2009	2454929.7	15.02 ± 0.04	14.85 ± 0.04	14.70 ± 0.04	RetroCam
11/4/2009	2454932.7	15.06 ± 0.04	14.92 ± 0.04	14.80 ± 0.04	RetroCam
14/4/2009	2454935.7	15.10 ± 0.04	15.11 ± 0.04	14.80 ± 0.04	RetroCam
16/4/2009	2454937.7	–	–	14.94 ± 0.04	RetroCam
18/4/2009	2454939.7	15.38 ± 0.04	15.23 ± 0.04	15.11 ± 0.04	RetroCam
24/4/2009	2454945.7	15.81 ± 0.04	15.65 ± 0.04	15.47 ± 0.04	RetroCam
27/4/2009	2454948.7	15.96 ± 0.04	15.84 ± 0.04	15.68 ± 0.05	RetroCam
28/4/2009	2454949.7	16.01 ± 0.04	15.95 ± 0.04	15.66 ± 0.05	RetroCam
24/5/2009	2454975.7	17.05 ± 0.04	17.23 ± 0.05	16.68 ± 0.08	RetroCam

Table 4: Optical peak light curve parameters

Filter	JD max ^a	m(obs) ^b	M(abs) ^c
<i>B</i>	2454921.0 ± 0.5	17.05 ± 0.02	−18.36 ± 0.44
<i>V</i>	2454923.5 ± 0.5	16.16 ± 0.02	−18.65 ± 0.34
<i>R</i>	2454924.1 ± 0.5	15.80 ± 0.01	−18.56 ± 0.28
<i>I</i>	2454926.5 ± 0.5	15.36 ± 0.03	−18.51 ± 0.21
<i>u'</i>	2454919.6 ± 0.5	18.04 ± 0.08	−17.68 ± 0.50
<i>g'</i>	2454921.9 ± 0.5	16.62 ± 0.02	−18.53 ± 0.40
<i>r'</i>	2454924.4 ± 0.5	15.96 ± 0.02	−18.60 ± 0.31
<i>i'</i>	2454925.5 ± 0.5	15.89 ± 0.02	−18.28 ± 0.25
<i>z'</i>	2454926.7 ± 0.5	15.60 ± 0.02	−18.27 ± 0.21
<i>Y</i>	2454929.8 ± 1.0	15.01 ± 0.05	−18.58 ± 0.19
<i>J</i>	2454928.4 ± 1.0	14.85 ± 0.05	−18.67 ± 0.18
<i>H</i>	2454929.2 ± 2.0	14.71 ± 0.06	−18.64 ± 0.17

^a JD time of peak brightness.

^b Apparent magnitude.

^c Absolute magnitude.

Table 5: Journal of spectroscopic observations

UT date	J.D.	epoch ^a (days)	range (Å)	res. (Å)	exptime (sec)	Instrument
28/03/09	2454918.7	−2.3	3800–9200	3.0	700	WFCCD
29/03/09	2454919.6	−1.4	3800–9200	3.0	900	WFCCD
03/04/09	2454924.6	3.6	3800–9200	3.0	700	WFCCD
07/04/09	2454928.5	7.5	4200–10000	1.9	400	IMACS
15/04/09	2454936.6	15.6	4200–8100	1.35	900	GMOS
17/04/09	2454938.6	17.6	3700–9300	2.0	600	LDSS3
18/04/09	2454939.6	18.6	3400–9500	3.0	700	B&C
22/04/09	2454943.6	22.6	3400–9500	3.0	900	B&C
23/04/09	2454944.6	23.6	3400–9500	3.0	1000	B&C
26/04/09	2454947.6	26.6	3900–8100	1.35	900	GMOS
30/04/09	2454938.6	30.6	3700–9300	2.0	600	LDSS3
14/05/09	2454965.5	44.5	4400–10000	1.9	600	IMACS
09/01/10	2455205.7	285.0	3700–9300	2.0	3x1800	LDSS3

^aRelative to *B*-band maximum.

Table 6: Mass of the elements used to generate the synthetic spectra in Figure 19.

Element	mass (M_{\odot})
O	1.06
Mg	0.012
Si	0.07
S	0.23
Ca	0.05
Ni	0.25

Table 7. *BVRI* photometry of the local photometric sequence

id	R.A.	Dec.	<i>B</i>	<i>V</i>	<i>R</i>	<i>I</i>
1	10:31:45.355	-40:00:42.73	15.26 ± 0.01	14.54 ± 0.04	14.13 ± 0.02	13.76 ± 0.01
2	10:31:44.107	-39:55:25.68	15.44 ± 0.02	14.47 ± 0.04	13.93 ± 0.03	13.41 ± 0.02
3	10:31:42.905	-39:57:51.19	13.83 ± 0.03	13.18 ± 0.03	12.80 ± 0.02	12.45 ± 0.01
4	10:31:41.494	-39:57:10.26	15.50 ± 0.02	14.53 ± 0.04	13.99 ± 0.02	13.49 ± 0.02
5	10:31:36.185	-39:54:45.04	14.98 ± 0.01	14.36 ± 0.03	13.99 ± 0.02	13.63 ± 0.02
6	10:31:24.828	-39:58:30.29	14.63 ± 0.01	14.12 ± 0.03	13.77 ± 0.01	13.42 ± 0.01
7	10:31:24.547	-40:01:44.72	15.00 ± 0.01	14.48 ± 0.04	14.14 ± 0.02	13.79 ± 0.01
8	10:31:50.942	-39:57:50.11	15.90 ± 0.01	15.04 ± 0.01	14.51 ± 0.03	14.02 ± 0.01
9	10:31:20.933	-39:59:52.55	15.83 ± 0.02	15.02 ± 0.01	14.57 ± 0.03	14.15 ± 0.01
10	10:31:48.010	-39:54:23.65	15.52 ± 0.01	14.96 ± 0.01	14.64 ± 0.02	14.29 ± 0.02
11	10:31:33.866	-40:00:09.68	15.86 ± 0.02	15.09 ± 0.01	14.69 ± 0.02	14.29 ± 0.01
12	10:31:26.273	-39:56:48.23	15.75 ± 0.01	15.10 ± 0.01	14.75 ± 0.01	14.38 ± 0.02
13	10:31:45.754	-39:56:32.17	15.84 ± 0.01	15.21 ± 0.01	14.86 ± 0.02	14.51 ± 0.03
14	10:31:51.468	-39:54:42.59	16.25 ± 0.01	15.52 ± 0.01	15.10 ± 0.03	14.68 ± 0.03
15	10:31:51.929	-39:54:27.94	16.36 ± 0.01	15.56 ± 0.01	15.11 ± 0.02	14.63 ± 0.04
16	10:31:24.012	-39:59:29.94	16.41 ± 0.02	15.62 ± 0.01	15.20 ± 0.03	14.78 ± 0.02
17	10:31:14.064	-39:58:45.55	16.45 ± 0.03	15.64 ± 0.01	15.19 ± 0.03	14.77 ± 0.01
18	10:31:16.582	-39:56:39.70	16.13 ± 0.04	15.62 ± 0.04	15.37 ± 0.05	15.06 ± 0.06
19	10:31:18.864	-39:57:51.30	16.55 ± 0.01	15.76 ± 0.01	15.33 ± 0.02	14.91 ± 0.01
20	10:31:23.846	-39:54:50.40	16.49 ± 0.02	15.80 ± 0.01	15.40 ± 0.02	15.01 ± 0.04
21	10:31:24.442	-39:55:08.33	16.79 ± 0.03	15.96 ± 0.01	15.49 ± 0.01	15.07 ± 0.03
22	10:31:46.673	-39:58:40.19	16.98 ± 0.01	16.28 ± 0.01	15.89 ± 0.02	15.50 ± 0.02
23	10:31:31.198	-39:53:32.46	17.52 ± 0.02	16.62 ± 0.01	16.06 ± 0.05	15.56 ± 0.02
24	10:31:49.822	-40:00:16.78	18.60 ± 0.01	17.08 ± 0.03	16.12 ± 0.06	15.04 ± 0.02
25	10:31:42.703	-39:58:20.78	17.56 ± 0.01	16.90 ± 0.01	16.50 ± 0.03	16.06 ± 0.03
26	10:31:48.434	-40:01:29.93	17.84 ± 0.02	17.14 ± 0.01	16.72 ± 0.05	16.32 ± 0.05
27	10:31:54.881	-39:56:16.58	19.25 ± 0.02	17.78 ± 0.01	16.77 ± 0.14	15.98 ± 0.10
28	10:31:33.463	-39:58:54.05	18.11 ± 0.02	17.45 ± 0.01	17.10 ± 0.04	16.71 ± 0.02
29	10:31:37.385	-39:57:52.78	18.83 ± 0.02	17.86 ± 0.01	17.35 ± 0.09	16.82 ± 0.04
30	10:31:32.995	-39:58:26.69	19.39 ± 0.02	18.22 ± 0.01	17.52 ± 0.04	16.76 ± 0.21
31	10:31:31.990	-39:58:28.85	18.86 ± 0.01	18.11 ± 0.01	17.64 ± 0.06	17.21 ± 0.06

Table 8. $u'g'r'i'z'$ photometry of the local photometric sequence

id	R.A.	Dec.	u'	g'	r'	i'	z'
1	10:31:45.355	-40:00:42.73	16.37 ± 0.06	14.83 ± 0.01	14.31 ± 0.02	14.14 ± 0.03	14.09 ± 0.02
2	10:31:44.107	-39:55:25.68	17.04 ± 0.07	–	14.13 ± 0.02	13.82 ± 0.03	13.71 ± 0.01
3	10:31:42.905	-39:57:51.19	–	–	12.96 ± 0.02	12.81 ± 0.03	12.81 ± 0.02
4	10:31:41.494	-39:57:10.26	17.20 ± 0.06	–	14.19 ± 0.02	13.91 ± 0.03	13.80 ± 0.04
5	10:31:36.185	-39:54:45.04	–	–	14.06 ± 0.02	13.91 ± 0.03	13.89 ± 0.04
6	10:31:24.828	-39:58:30.29	–	–	13.91 ± 0.02	13.76 ± 0.03	13.75 ± 0.01
7	10:31:24.547	-40:01:44.72	15.82 ± 0.02	14.68 ± 0.01	14.31 ± 0.02	14.16 ± 0.03	14.14 ± 0.03
8	10:31:50.942	-39:57:50.11	17.25 ± 0.05	15.41 ± 0.01	14.71 ± 0.01	14.43 ± 0.01	14.32 ± 0.05
9	10:31:20.933	-39:59:52.55	17.15 ± 0.07	15.37 ± 0.01	14.76 ± 0.01	14.56 ± 0.01	14.52 ± 0.02
10	10:31:48.010	-39:54:23.65	16.38 ± 0.04	15.19 ± 0.01	14.79 ± 0.01	14.65 ± 0.01	14.66 ± 0.06
11	10:31:33.866	-40:00:09.68	17.09 ± 0.06	15.41 ± 0.01	14.86 ± 0.01	14.67 ± 0.01	14.67 ± 0.06
12	10:31:26.273	-39:56:48.23	16.69 ± 0.04	15.37 ± 0.01	14.91 ± 0.01	14.76 ± 0.01	14.73 ± 0.04
13	10:31:45.754	-39:56:32.17	16.83 ± 0.05	15.47 ± 0.01	15.03 ± 0.01	14.88 ± 0.01	14.96 ± 0.07
14	10:31:51.468	-39:54:42.59	17.24 ± 0.04	15.83 ± 0.01	15.28 ± 0.01	15.06 ± 0.01	15.03 ± 0.04
15	10:31:51.929	-39:54:27.94	17.55 ± 0.05	15.90 ± 0.01	15.29 ± 0.01	15.03 ± 0.01	14.95 ± 0.02
16	10:31:24.012	-39:59:29.94	17.70 ± 0.06	15.96 ± 0.01	15.34 ± 0.01	15.14 ± 0.01	14.88 ± 0.04
17	10:31:14.064	-39:58:45.55	17.76 ± 0.05	15.99 ± 0.01	15.39 ± 0.01	15.18 ± 0.01	15.11 ± 0.03
18	10:31:16.582	-39:56:39.70	16.94 ± 0.11	15.86 ± 0.11	15.45 ± 0.05	15.32 ± 0.06	15.37 ± 0.04
19	10:31:18.864	-39:57:51.30	17.60 ± 0.03	16.08 ± 0.01	15.51 ± 0.01	15.31 ± 0.01	15.24 ± 0.04
20	10:31:23.846	-39:54:50.40	17.52 ± 0.04	16.09 ± 0.01	15.60 ± 0.01	15.42 ± 0.01	15.43 ± 0.08
21	10:31:24.442	-39:55:08.33	18.08 ± 0.06	16.32 ± 0.01	15.70 ± 0.01	15.49 ± 0.01	15.52 ± 0.06
22	10:31:46.673	-39:58:40.19	18.06 ± 0.05	16.57 ± 0.01	16.07 ± 0.01	15.90 ± 0.01	15.89 ± 0.08
23	10:31:31.198	-39:53:32.46	18.99 ± 0.13	17.02 ± 0.01	16.29 ± 0.01	16.00 ± 0.01	15.96 ± 0.08
24	10:31:49.822	-40:00:16.78	20.87 ± 0.17	17.81 ± 0.01	16.44 ± 0.01	15.61 ± 0.01	15.29 ± 0.06
25	10:31:42.703	-39:58:20.78	18.47 ± 0.06	17.18 ± 0.01	16.70 ± 0.01	16.50 ± 0.01	16.75 ± 0.45
26	10:31:48.434	-40:01:29.93	18.87 ± 0.03	17.42 ± 0.01	16.90 ± 0.01	16.72 ± 0.01	16.73 ± 0.22
27	10:31:54.881	-39:56:16.58	–	18.50 ± 0.01	17.14 ± 0.01	16.42 ± 0.01	16.04 ± 0.08
28	10:31:33.463	-39:58:54.05	19.05 ± 0.05	17.73 ± 0.01	17.25 ± 0.01	17.07 ± 0.01	17.54 ± 0.92
29	10:31:37.385	-39:57:52.78	20.41 ± 0.08	18.31 ± 0.01	17.46 ± 0.01	17.16 ± 0.01	17.91 ± 0.46
30	10:31:32.995	-39:58:26.69	–	18.76 ± 0.01	17.66 ± 0.01	17.26 ± 0.01	16.98 ± 0.45
31	10:31:31.990	-39:58:28.85	19.97 ± 0.13	18.44 ± 0.01	17.85 ± 0.01	17.63 ± 0.01	17.19 ± 0.43

Table 9. YJH photometry of the local photometric sequence

id	R.A.	Dec.	Y	J	H
1	10:31:45.355	-40:00:42.73	12.23 ± 0.01	11.99 ± 0.01	11.70 ± 0.01
2	10:31:44.107	-39:55:25.68	12.78 ± 0.01	12.57 ± 0.01	12.34 ± 0.02
3	10:31:42.905	-39:57:51.19	13.03 ± 0.01	12.69 ± 0.01	12.19 ± 0.01
4	10:31:41.494	-39:57:10.26	13.11 ± 0.01	12.76 ± 0.01	12.29 ± 0.02
5	10:31:36.185	-39:54:45.04	13.21 ± 0.01	12.97 ± 0.01	12.68 ± 0.01
6	10:31:24.828	-39:58:30.29	13.22 ± 0.01	12.85 ± 0.01	12.37 ± 0.02
7	10:31:24.547	-40:01:44.72	13.55 ± 0.01	13.27 ± 0.01	12.92 ± 0.01
8	10:31:50.942	-39:57:50.11	13.41 ± 0.01	13.16 ± 0.01	12.87 ± 0.03
9	10:31:20.933	-39:59:52.55	13.69 ± 0.01	13.32 ± 0.01	12.75 ± 0.01
10	10:31:48.010	-39:54:23.65	13.59 ± 0.01	13.29 ± 0.01	12.86 ± 0.01
11	10:31:33.866	-40:00:09.68	13.73 ± 0.01	13.45 ± 0.01	13.14 ± 0.01
12	10:31:26.273	-39:56:48.23	13.71 ± 0.01	13.35 ± 0.01	12.84 ± 0.01
13	10:31:51.468	-39:54:42.59	13.83 ± 0.01	13.42 ± 0.01	12.88 ± 0.01
14	10:31:51.929	-39:54:27.94	13.97 ± 0.01	13.69 ± 0.01	13.39 ± 0.02
15	10:31:24.012	-39:59:29.94	14.05 ± 0.01	13.75 ± 0.01	13.42 ± 0.01
16	10:31:14.064	-39:58:45.55	14.15 ± 0.01	13.90 ± 0.01	13.59 ± 0.01
17	10:31:16.582	-39:56:39.70	14.28 ± 0.01	14.00 ± 0.01	13.71 ± 0.01
18	10:31:18.864	-39:57:51.30	14.21 ± 0.01	13.80 ± 0.01	13.28 ± 0.01
19	10:31:23.846	-39:54:50.40	14.30 ± 0.01	14.05 ± 0.01	13.76 ± 0.01
20	10:31:24.442	-39:55:08.33	14.24 ± 0.01	14.00 ± 0.01	13.73 ± 0.02
21	10:31:46.673	-39:58:40.19	14.29 ± 0.01	13.97 ± 0.01	13.58 ± 0.02
22	10:31:31.198	-39:53:32.46	14.39 ± 0.01	14.10 ± 0.01	13.71 ± 0.02
23	10:31:49.822	-40:00:16.78	14.48 ± 0.01	14.02 ± 0.01	13.35 ± 0.01
24	10:31:42.703	-39:58:20.78	14.54 ± 0.01	14.24 ± 0.01	13.90 ± 0.01
25	10:31:48.434	-40:01:29.93	14.77 ± 0.01	14.49 ± 0.01	14.15 ± 0.01
26	10:31:54.881	-39:56:16.58	14.74 ± 0.01	14.23 ± 0.01	13.67 ± 0.01
27	10:31:33.463	-39:58:54.05	15.09 ± 0.01	14.82 ± 0.01	14.48 ± 0.02
28	10:31:37.385	-39:57:52.78	15.25 ± 0.01	14.95 ± 0.01	14.71 ± 0.01
30	10:31:32.995	-39:58:26.69	15.72 ± 0.01	15.24 ± 0.01	14.70 ± 0.01
29	10:31:31.990	-39:58:28.85	15.63 ± 0.01	15.12 ± 0.01	14.57 ± 0.02
31	10:31:21.082	-39:58:30.44	15.84 ± 0.01	15.56 ± 0.01	15.30 ± 0.03

